A NOVEL MODEL OF ELEVATED MITOCHONDRIAL CHOLESTEROL AND THE CONSEQUENCES FOR MITOCHONDRIAL FUNCTION

By

Luke Hattie

Submitted in partial fulfilment of the requirements
for the degree of Master of Science

at

Dalhousie University
Halifax, Nova Scotia
August 2019

TABLE OF CONTENTS

LIST OF TABLES

LIST OF FIGURES

ABSTRACT

Increased mitochondrial cholesterol may induce mitochondrial dysfunction and play a role in the progression of neurodegenerative disease and cancer. The voltage-dependent anion channel of the outer mitochondrial membrane has been proposed to participate in cholesterol-related mitochondrial dysfunction through altered associations with proteins involved in metabolism and apoptosis. Current models for studying the effects of mitochondrial cholesterol are disease-based models, blurring the line between true mitochondrial cholesterol effects and other disease effects. Here we present a novel model of increased mitochondrial cholesterol, MitoSTARD4, in which mitochondrial cholesterol content and import to the inner mitochondrial membrane are increased. Cells with increased mitochondrial cholesterol produce more lactate. I explored the mitochondrial associations of voltage-dependent anion channel interacting proteins in cells with elevated mitochondrial cholesterol; BCL-XL, GRP75, PINK1 and PARKIN all have increased mitochondrial presence. The MitoSTARD4 model supports previous findings in disease models that increased mitochondrial cholesterol content induces alterations to mitochondrial function.

LIST OF ABBREVIATIONS USED

22-OH Chol	22-Hydroxycholesterol
ANOVA	Analysis of variance
ANT	Adenine nucleotide transporter
BCL-XL	B-cell lymphoma, extra large
BSA	Bovine serum albumin
CHO	Chinese hamster ovary
DCA	Dichloroacetate
DMEM	Dulbecco's modified eagles medium
EDTA	Ethylenediaminetetraacetic acid
ER	Endoplasmic reticulum
F2	CYP11A1, ferredoxin reductase, and ferredoxin 1 fusion protein
FBS	Fetal bovine serum
FFAT	Two phenylalanines in an acidic tract
FKBP	FK506 binding protein
FRB	FKBP12 rapamycin-binding domain
GRP75	Glucose-regulated protein 75
HDR	Homology-directed repair
HEK	Human embryonic kidney
HMGCR	3-hydroxy-3-methylglutaryl-CoA reductase
HRP	Horseradish peroxidase
HXK1	Hexokinase 1
HXK2	Hexokinase 2
LDL	Low-density lipoprotein
MEM	Minimal essential media
MENTAL	MLN64 N-terminal domain
NAC	N-acetyl cysteine
NPC	Niemann-Pick Type C
NPC1	Niemann-Pick Type C1
NPC2	Niemann-Pick Type C2
NRF2	Nuclear factor erythroid 2-related factor 2
PAGE	Polyacrylamide gel electrophoresis
PBS	Phosphate buffered saline
PCR	Polymerase chain reaction
PCTP	Phosphatidylcholine transfer protein
PDH	Pyruvate dehydrogenase
PEI	Polyethyleneimine
PINK1	PTEN-induced kinase 1
qPCR	Quantitative polymerase chain reaction
RIA	Radioimmunoassay
ROS	Reactive oxygen species
SCAP	SREBP cleavage activating protein
SDS	Sodium dodecyl sulfate

sgRNA	Single guide RNA
SREBP	Sterol regulatory element binding protein
StAR	Steroidogenic acute regulatory
STARD1	StAR-related lipid transfer domain protein 1
STARD3/MLN64	StAR-related lipid transfer domain protein 3, metastatic lymph node 64
STARD4	StAR-related lipid transfer domain protein 4
STARD5	StAR-related lipid transfer domain protein 5
START	StAR-related lipid transfer
TBS	Tris buffered saline
TCA	Tricarboxylic acid cycle
TOMM20	Translocase of outer mitochondrial membrane 20
TTBS	Tris buffered saline + Tween20
VDAC	Voltage-dependent anion channel
WT	Wildtype
YFP	Yellow fluorescent protein

ACKNOWLEDGEMENTS

First of all, I would like to thank my supervisor, Dr. Barbara Karten. Working in the Karten lab for the past two years has been both an enjoyable and rewarding experience. Barbara always fostered a friendly, collaborative environment in her lab. Barbara is extraordinarily committed to both her work and to the people that are in her lab. She is always there for input and advice and is a great teacher. I have learned so much in my time in the Karten lab, and she has helped me immensely with my work. I am very appreciative that I had the chance to work with a supervisor who is as friendly, supportive, and patient as Barbara has been.

I also want to thank Aaron Woblistin, a PhD candidate also from the Karten lab. Through these two years, he has provided lots of insight into issues and questions regarding my project. Aaron started before I did in the Karten lab, and when I began, he was a huge help with learning new-to-me techniques and the ways of the lab. Aaron was great to work with, easy to get along with, and when I started here at Dalhousie, he introduced me to many people that I consider great friends now.

Next, I want to thank Lynn Thomas, a technician in the Karten lab, who has also been a great help and wonderful to work with. Lynn is always great to turn to for help with things in the lab, she is always friendly and always smiling. Lynn is always great to talk to, supportive and encouraging.

Current and former members of the Karten lab, Madhav Makkena, Shawna Dexter, Lindsay Cormier, and Victoria Palmgren, have all been wonderful to work with, provided valuable insight and helped build the friendly, enjoyable atmosphere working in the Karten lab.

My committee members, Dr. Neale Ridgway and Dr. Aarnoud Van Der Spoel, have been knowledgeable, supportive and encouraging. They are both very approachable, understanding and I appreciate their contributions to my progress.

I also thank the many other friends I have made over my time at Dalhousie, most of whom are other graduate students going through the same things. To only name a few; Dane, Patrick, Michal, Alexa, Isa, Lucas, have all made my time here much more enjoyable.

Finally, I certainly couldn't have done any of this without the support of my amazing Fiancée, Bailey McNutt. It makes a huge difference having someone that's as supportive, understanding, patient, and encouraging as Bailey has been.

CHAPTER 1: INTRODUCTION

1.1 Cellular Cholesterol Homeostasis

1.1.1 Functions of Cholesterol

Cholesterol is an important lipid present in all animal cell membranes. Cholesterol influences the physical properties of a membrane and interacts with membrane proteins. Cholesterol within a lipid bilayer induces conformational ordering of fatty acyl chains, increasing packing and extends the temperature range at which a membrane is fluid (Bloom, Evans and Mouritsen, 1991). Cholesterol also reduces the permeability of a membrane to potassium, sodium and hydrogen ions, maintaining membrane ion potentials (Haines, 2001).

Cholesterol is a precursor to oxysterols, steroid hormones, and bile acids (Rennert et al., 1990, Spady et al., 1989), which have roles in endocrine homeostasis and absorption of cholesterol from the digestive tract, respectively. Cholesterol also forms nanodomains with sphingolipids which may participate in signal transduction and endocytosis (Pike, 2003).

Cholesterol is enriched in the brain by roughly 5-fold over other tissues, mostly in the myelin sheaths that surround axons (Vance, 2012). Cholesterol content of brain myelin is 20-30% of total lipid weight, second only to phospholipids for percent composition (Norton and Autilio, 1965, Evans and Finean, 1965). Neurons in particular have a high cholesterol requirement for synaptogenesis and dendrite formation (Mauch et al., 2001, Goritz et al., 2005). Dysfunctional

cholesterol homeostasis is associated with neurodegenerative diseases (Vance, 2012, Arenas et al., 2017, Torres et al., 2017). However, the mechanisms by which cholesterol contributes to neurodegenerative disease progression are not fully understood.

1.1.2 Subcellular Cholesterol Distribution

Cholesterol is the main non-polar lipid in mammalian cell membranes. Cholesterol is synthesized by all animal cells; however, the subcellular distribution of cholesterol is highly varied. Membrane composition of cholesterol is largely determined by the other lipid components of the membrane, the headgroups of phospholipids and degree of acyl chain saturation. Cholesterol's relatively small hydroxyl group leaves the hydrophobic ring structure to be exposed to water, while large polar headgroups on surrounding lipids provide protection from water and cholesterol will less readily leave the membrane (Mesmin and Maxfield, 2009). Hence, cholesterol is more protected in membranes composed of phospholipids with large polar headgroups like phosphatidylcholine and sphingomyelin and less protected by diacylglycerols, ceramides and phosphatidylethanolamine (Mesmin and Maxfield, 2009). Nearby phospholipid head groups thus influence the disassociation and extractability of cholesterol from membranes, which is an important factor in the trafficking of cholesterol between membranes. The stability of cholesterol in a membrane is largely influenced by the degree of unsaturation of surrounding acyl chains. Cholesterol is a four-ringed planar structure with a large hydrophobic region. Given the rigidity of the planar rings, cholesterol packs tightly

with unsaturated acyl chains, increasing interactions and membrane stability (Pan, Tristram-Nagle and Nagle, 2009, Silvius, 2003). Cholesterol distribution is modulated by these lipid interactions, as cholesterol which is more protected from the aqueous phase is more accessible to cholesterol transport proteins, and a tighter association with other lipids increases the affinity of cholesterol to a given membrane.

The plasma membrane has the highest cholesterol content, comprising approximately 50% of total lipids (Meer, Voelker, and Feigenson, 2008). Intracellularly, cholesterol is sparser, with 5% to 20% of membrane lipids being cholesterol (van Meer, Voelker, and Feigenson, 2008). Cholesterol content is lowest at the endoplasmic reticulum (ER), which is also the site of cholesterol sensing, synthesis and esterification. Low ER cholesterol is maintained as cholesterol is rapidly trafficked to other membranes or converted to cholesteryl esters for storage in lipid droplets. Most cholesterol synthesized at the ER is transported to the plasma membrane, to the Golgi apparatus, or is esterified and stored in lipid droplets. The Golgi apparatus increases in cholesterol content from the cis-Golgi to the trans-Golgi network and out to the plasma membrane (Liscum and Munn, 1999). Cholesterol originating from extracellular sources enters the endocytic pathway, with early endosomes having a similar cholesterol content to the plasma membrane. Endosomal cholesterol is sorted to the endocytic recycling compartment or trafficked back to the plasma membrane, reducing endosomal cholesterol as they mature.

1.1.3 Cholesterol Sensing, Synthesis, and Uptake

Cholesterol and fatty acid synthesis are controlled by the sterol regulatory element binding protein (SREBP) family of basic helix-loop-helix leucine zipper transcription factors. There are three SREBP isoforms, SREBP1-a, SREBP1-c, and SREBP2, which are synthesized as inactive precursor proteins and span the ER membrane (Hua et al., 1995-1, Brown and Goldstein, 1997, Horton et al., 2002). These precursor proteins are each composed of three domains; an amino terminal helix-loop-helix nuclear transcription domain, two transmembrane regions, and a carboxy terminal regulatory domain (Hua et al., 1993, Hua et al., 1995). The nuclear transcription domain and regulatory domain both reside on the cytosolic side of the ER membrane (Hua et al., 1995). Activation of SREBPs requires cleavage of the nuclear domain from the transmembrane domain, allowing translocation to the nucleus and activation of sterol response element (SRE) regulated genes (Briggs et al., 1993, Hua et al., 1993, Hua et al, 1996), this cleavage is regulated by ER-cholesterol levels as described below. SREBP1 and SREBP1c regulate *de novo* fatty acid synthesis, and SREBP2 regulates cholesterol synthesis and uptake (Hua et al., 1995-2, Horton et al., 2003).

SREBP2 is retained in the ER membrane when sterol levels are high through complex formation with SREBP cleavage-activating protein (SCAP) and insulin-induced gene 1 (INSIG1). SCAP functions as the cholesterol sensor for SREBP2 (Nohturfft et al., 1998). SCAP contains a sterol sensing domain; cholesterol binding to SCAP inhibits COPII protein binding and vesicular transport to the Golgi, through

interaction with INSIG1 (Espenshade et al., 2002). Under conditions of low cholesterol, the SCAP-INSIG1 complex dissociates, COPII proteins bind to SCAP, and transport SCAP and SREBP to the Golgi. In the Golgi, Site 1 protease (S1P) cleaves SREBP between the two transmembrane domains and the two terminal domains remain bound to the Golgi membrane (Brown and Goldstein, 1999). Site 2 protease (S2P) cleaves the nuclear transcription domain from the transmembrane domain (Brown and Goldstein, 1999). The transcription factor domain of SREBP2 dimerizes, translocates to the nucleus and activates genes containing an SRE.

Synthesis of cholesterol from acetyl-CoA requires the coordination of over 40 enzymes. SREBP2 regulates the expression of nearly all of these enzymes including HMG-CoA reductase. HMG-CoA reductase catalyzes a key regulatory step in the mevalonate pathway (Sakakura et al., 2001), which results in the production of isoprenoids. Isoprenoids are precursors to the formation of thousands of biomolecules, including cholesterol, heme, and farnesyl and geranyl-geranyl moieties for protein prenylation. The isoprenoids produced by the mevalonate pathway continue into the steroid synthesis pathway, where six isoprenoid units are joined to form squalene, and eventually leads to cholesterol synthesis.

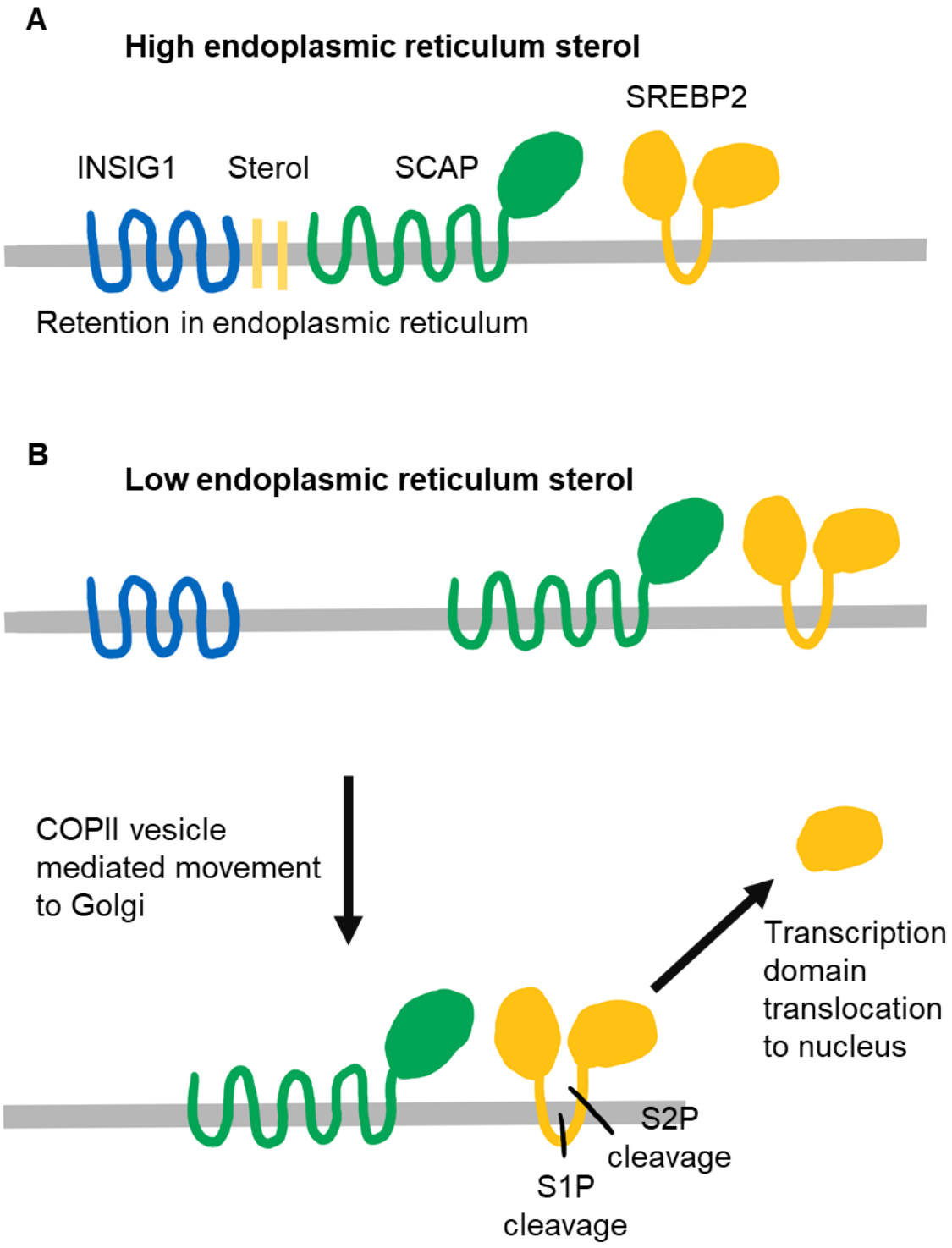
A
High endoplasmic reticulum sterol
SREBP2
INSIG1
Sterol
SCAP
Retention in endoplasmic reticulum
B
Low endoplasmic reticulum sterol
COPII vesicle
mediated movement
to Golgi
Transcription
domain
translocation
to nucleus
S2P
cleavage
S1P
cleavage

Figure 1.01 **SREBP2 Activation**
A) Depiction of sterol-mediated retention of SREBP2 in the ER membrane by INSIG1 and SCAP. B) Low ER cholesterol content induces dissociation of INSIG1 and SCAP, translocation of SCAP and SREBP2 to the Golgi in COPII vesicles. Proteases S1P and S2P cleave the nuclear transcription domain of SREBP2, which then translocates to the nucleus.

HMG-CoA reductase is regulated on the transcriptional level by SREBP2 and through rapid degradation of the protein when cholesterol levels are high. Sterol binding to INSIG1 leads to complex formation with HMG-CoA reductase, subsequent ubiquitination and proteasomal degradation of HMG-CoA reductase (Sever et al., 2003). By reducing the production of HMG-CoA reductase and increasing its degradation, cholesterol synthesis is reduced. In addition, HMG-CoA reductase is inhibited by phosphorylation, which is an important regulatory mechanism to down-regulate cholesterol synthesis in response to glucagon and low energy levels (Ness, Zhao, Wiggins, 1994). HMG-CoA reductase activity is inhibited by the statin class of drugs, reducing the rate of cholesterol synthesis.

Dietary cholesterol and cholesterol produced by hepatocytes is distributed through the vascular system in lipoproteins. The low-density lipoprotein (LDL) receptor binds LDL on the cell surface for uptake via endocytosis. By mass, LDL are over 50% composed of cholesteryl esters and free cholesterol, SREBP2 activation increases LDL receptor synthesis, increasing LDL uptake and cellular cholesterol (Kuchinskiene and Carlson, 1982, Streicher et al., 1996). LDL is internalized through receptor-mediated endocytosis and delivered to the late endosome, while the LDL receptor is recycled back to the cell surface. The distribution of cholesterol from late endosomes will be described in section 1.3.1.

1.2 Mitochondrial Cholesterol Trafficking: Role of the START-Protein Family

1.2.1 START-Protein Family

The role of cholesterol in mitochondrial membranes is presumably the same as its role in other membranes, regulating curvature and fluidity of the membrane and its permeability to ions. Cholesterol trafficking to mitochondria is likely covered by redundant pathways, the best-known pathway is mediated by steroidogenic acute regulatory protein (StAR) in steroidogenic cells. StAR is a member of StAR-related lipid transfer- (START) protein family of lipid transporters, and other members of the START-protein family have been implicated in mitochondrial cholesterol transport as well.

The STARD family is composed of 15 members, STARD1-STARD15, that are involved in lipid transport and signaling. The START domain is a ~210 residue hydrophobic lipid-binding pocket common among STARD members. The family was originally identified upon sequence comparison of STARD1 and STARD3, finding the similar carboxy terminal START domain. Steroidogenic acute regulatory protein (StAR/STARD1) was the first member and the namesake of the family, initially found to be expressed in response to luteinizing hormone stimulation and essential for steroidogenesis (Clarke et al., 1995). The STARD1/STARD3 and STARD4 subfamilies are cholesterol-binding members of the larger family and are involved in cellular cholesterol homeostasis. The remaining members of the family have

binding specificity for phosphatidylcholine, phosphatidylethanolamine or ceramides (Wirtz, 1991, Olaioye et al., 2005, Soccio et al., 2005, Hanada et al., 2005).

The START domain crystal structure has been solved for STARD3 and STARD4, revealing a hydrophobic pocket large enough to accommodate a sole cholesterol molecule, as well as a hinged carboxyl terminal lid domain (Tsujishita and Hurley, 2000, Romanowski et al., 2002). Due to the hydrophobic nature of cholesterol, the lid of START domains is believed to further shield the ligand within the hydrophobic pocket from the aqueous environment. Removal of the lid domain by truncation of the carboxyl terminus of STARD1 or phosphatidylcholine transfer protein (PCTP/STARD2) abolishes ligand transfer (Arkane et al., 1996, Feng et al., 2000).

1.2.2 STARD1-Mediated Mitochondrial Cholesterol Import

Steroidogenic cells require cholesterol for the synthesis of steroid hormones, which begins with cholesterol import into mitochondria. CYP450scc (CYP11A1) resides at the inner mitochondrial membrane and catalyzes the conversion of cholesterol to pregnenolone, a precursor to all steroid hormones (Simpson, 1979). Cholesterol arrival at the inner mitochondrial membrane is the rate-limiting step in steroid hormone synthesis (Young and Hall, 1968). STARD1 has a mitochondrial targeting sequence and was originally identified to be acutely upregulated in response to luteinizing hormone stimulation of mouse MA-10 Leydig tumor cells (Clark et al., 1994). STARD1 overexpression increased steroidogenesis in the absence of luteinizing hormone stimulation (Clark and Stocco, 1995). Regulation of

the expression of STARD1 regulates the rate of steroidogenesis, as STARD1 is the main protein responsible for the import of cholesterol from the outer mitochondrial membrane to the inner mitochondrial membrane.

The mechanism of STARD1-mediated mitochondrial cholesterol import is not known in detail. STARD1 is imported into mitochondria and proteolytically processed into 32 and 30 kDa forms and it was proposed that processing and import of STARD1 was required for cholesterol import, and STARD1 acted as a cholesterol shuttle (Clark et al., 1994). It was later found that N-terminal truncated STARD1 with no mitochondrial targeting sequence was not imported into mitochondria, but still maintained cholesterol import (Clark et al., 1994, Clark and Stocco, 1996). Further studies showed that a fusion protein targeting STARD1 to the outer mitochondrial membrane supported cholesterol import, but not when targeted to the inner mitochondrial membrane or inter-membrane space (Bose et al., 2002). It was later found that STARD1 mitochondrial import is not necessary for cholesterol import, but STARD1 needs to be processed to the 30 kDa form and imported to the inner mitochondrial membrane to achieve full cholesterol import activity (Artemenko et al., 2001). A large mitochondrial protein complex of Voltage-dependent anion channel 1 (VDAC1), translocator protein, ATPase family AAA-domain containing protein 3A, and CYP11A1 was identified by photocholesterol crosslinking in hormone-stimulated cells (Rone et al., 2012). STARD1 and VDAC1 also interact (Bose et al., 2008). Formation of this intermembrane space-crossing protein complex is currently thought to be the mechanism by which cholesterol is

imported from extramitochondrial sources, into the inner mitochondrial membrane (Lacapere and Papadopoulos, 2003, Rone et al., 2012, Issop et al., 2012).

STARD1 likely mediates transport of cholesterol to mitochondria from ER and lipid droplets, possibly at contact sites. Inhibition of endogenous cholesterol synthesis greatly reduces steroid production in steroidogenic cells, which is also achieved by depletion of STARD1 (Montero et al., 2008, Morales et al., 2011), suggesting that ER contact is required to maintain cholesterol import through STARD1. Lipid droplets are commonly found in steroidogenic cells and can be found in close association with mitochondria (Kraemer et al., 2013, Zehmer et al., 2009, Almahbobi et al., 2009), and it lipid droplets may provide cholesterol to support steroidogenesis.

1.2.3 STARD3, an Endosomal START-Protein

STARD3 is a late endosomal perimeter membrane protein containing a START domain and a two phenylalanines in an acidic tract (FFAT) motif on the cytosolic side (Alpy et al., 2001). STARD3 is anchored in membrane via a membrane-spanning, cholesterol binding MLN64 N terminal (MENTAL) domain, which is involved in cholesterol movement between the membrane and the START domain (Alpy et al., 2005). The ER and late endosomes form contact sites via interaction between VAP on the ER and the FFAT motif on STARD3. These contact sites mediate the transfer of ER cholesterol to the late endosome (Alpy et al., 2013, Wilhelm et al., 2017). Depletion of STARD3 reduces cholesterol import to the inner mitochondrial membrane (Charman et al., 2010) and import occurs in semi-

permeabilized cells, indicating that STARD3 mediates the transfer of cholesterol to inner mitochondrial membrane without cytosolic transport proteins (Kennedy, Charman, Karten, 2012). Depletion of endosomal cholesterol by incubation in lipoprotein deficient serum followed by supplementation with LDL increases mitochondrial cholesterol import sooner than ER cholesterol is replenished, suggesting that STARD3 transfers cholesterol directly to mitochondria, not through the ER (Kennedy, Charman, Karten, 2012). The mechanism of cholesterol transport to mitochondria is not fully known, but it has been suggested that STARD3 may be involved in an import complex similar to STARD1.

1.2.4 STARD4, a Cytosolic Cholesterol Transport Protein

The STARD4 subfamily includes STARD4, STARD5 and STARD6, all of which bind cholesterol or other sterols. These proteins have a START domain but lack a targeting sequence and have 32-36% identity with each other (Soccio et al., 2002). Both STARD4 and STARD5 are expressed in all tissues, but highest in the liver and kidney, respectively (Soccio et al., 2002). STARD5 binds bile-acids and is upregulated in response to ER stress (Létourneau et al., 2012, Soccio et al., 2005, Rodriguez-Agudo et al., 2012). STARD6 is expressed solely in the testis (Gomes et al., 2005). StARD4 expression is regulated by cellular cholesterol levels through SREBP2 (Soccio et al., 2005, Rodriguez-Agudo et al., 2011). STARD4 overexpression increases cholesterol esterification, transfer to lipid droplets, formation of bile acids, and synthesis of progesterone (Rodriguez-Agudo et al., 2008, Rodriguez-Agudo et al., 2011, Soccio et al., 2005). Overexpression of STARD4 also increases delivery of

cholesterol from the plasma membrane to the endocytic recycling compartment (Iaea et al., 2017). Cholesterol redistribution induced by ectopic STARD4 expression can be mimicked with cellular injection of β-cyclodextrin, which binds and transports cholesterol in an unspecific manner (Iaea et al., 2017). This suggests that STARD4 is not targeted to traffic cholesterol between specific organelles, but rather shuttles cholesterol based on membrane lipid content, the stability of cholesterol in the membrane and its extractability.

1.3 Cholesterol-Related Mitochondrial Dysfunction

1.3.1 NPC Disease and Mitochondrial Cholesterol

Niemann-Pick Type C (NPC) is an autosomal recessive neurovisceral lysosomal storage disease caused by mutations to the *NPC1* or *NPC2* genes, disrupting cellular cholesterol trafficking. *NPC1* mutations cause 95% of cases, and *NPC2* gene mutations causes the other 5% (Carstea et al., 1993, Carstea et al., 1997). NPC disease occurs in one out of 120,000 live births (Vanier and Millat, 2003). Affected individuals have widespread neurological abnormalities, that begin as developmental deficits in early childhood. Purkinje neurons in the cerebellum are lost as the disease progresses, leading to the development of cerebellar ataxia, mental regression, and dystonia (Vanier et al., 1991). Accumulation of cholesterol occurs in various tissues of NPC patients, causing hepatosplenomegaly in many cases, which is the enlargement of liver and spleen (Patterson et al., 2001).

Niemann-Pick Type C protein 1 (NPC1) is a late endosomal perimeter membrane protein that participates in cholesterol trafficking from endosomes to the

plasma membrane and the ER (Millard et al., 2000, Karten et al., 2009, Ory, 2004) (Figure 1.02 A). Loss of NPC1 or dysfunctional NPC1 leads to the accumulation of cholesterol and glycolipids in late endosomes and lysosomes, and elevation of mitochondrial cholesterol levels (Figure 1.02 B) (Sokol et al., 1988, Charman et al., 2010, Fernandez et al., 2009). Niemann-Pick Type C protein 2 (NPC2) resides within the lumen of endosomes, and interacts with NPC1 (Deffieu and Pfeffer, 2011). NPC2 has a cholesterol binding pocket and is believed to retrieve cholesterol from internal membranes of multivesicular late endosomes and hand-off cholesterol to NPC1 (Figure 1.02 A) (Xu et al., 2007, Infante et al., 2008, Kwon et al., 2009). Dysfunctional NPC2 also causes endosomal and lysosomal accumulation of cholesterol and glycolipids seen in NPC disease, as hand-off to NPC1 is abolished (Figure 1.02 C) (Naureckiene et al., 2000).

Besides cholesterol, sphingolipids accumulate in endosomes and lysosomes in NPC disease and some therapies aimed to target this accumulation. An inhibitor of glucosylceramide synthase, Miglustat, reduces sphingolipid accumulation and delayed disease progression in mice (Zervas et al., 2001). Miglustat therapy has not proven as effective in human NPC patients, some symptoms were improved for a period of time, such as dystonia and dysarthria, but developmental delay and cognitive impairment were not improved (Fecarotta et al., 2015). While there has been some efficacy in miglustat trials, it only addresses one smaller aspect of NPC disease, and not cholesterol accumulation.

Elevated mitochondrial cholesterol increases oxidative stress, in part due to impaired glutathione import (Mari et al., 2006, Mari et al., 2009). Glutathione is an antioxidant vital to the counteraction of reactive oxygen species (ROS) produced by the electron transport chain in the mitochondria. Elevated ROS are present in mitochondria in the NPC1-deficient Chinese hamster ovary (CHO) cell line 4-4-19 (Kennedy et al., 2014). NRF2, a transcription factor controlling the oxidative stress response, is upregulated in NPC1-depleted CHO cells (Kennedy et al., 2014). Co-depletion of STARD3 and NPC1 in CHO cells reduces mitochondrial cholesterol accumulation compared to NPC1 depletion alone (Charman et al, 2010). NRF2 levels are unchanged with depletion of STARD3 or co-depletion of STARD3 and NPC1 (Kennedy et al., 2014). Furthermore, treatment of cells with N-acetyl cysteine (NAC), a precursor to the antioxidant glutathione, reduces NRF2 expression in NPC1 depleted cells compared to that of control (Kennedy et al., 2014). NPC1 null mice also show an increase in NRF2 expression, as well increased expression of some NRF2 target genes (Kennedy et al., 2013). These studies indicate that NRF2 increase was caused by mitochondrial cholesterol, as it was prevented by the co-depletion of STARD3.

Functional NPC1, NPC2 proteins

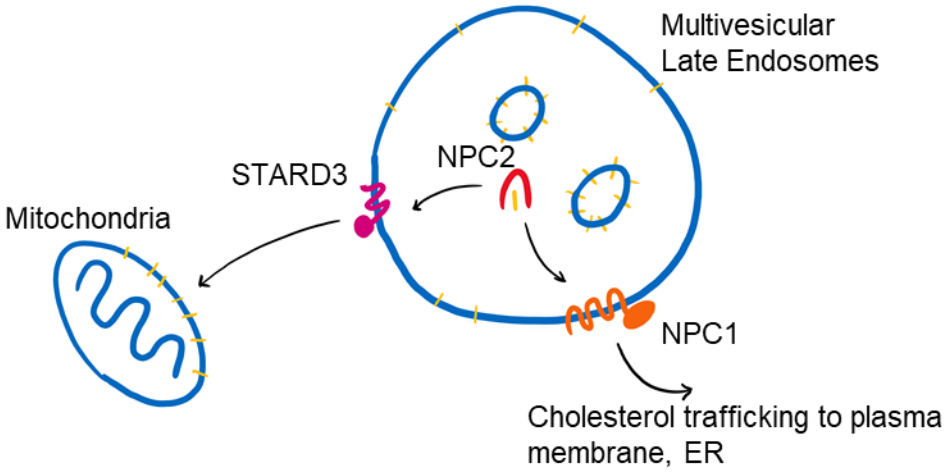

Dysfunctional NPC1

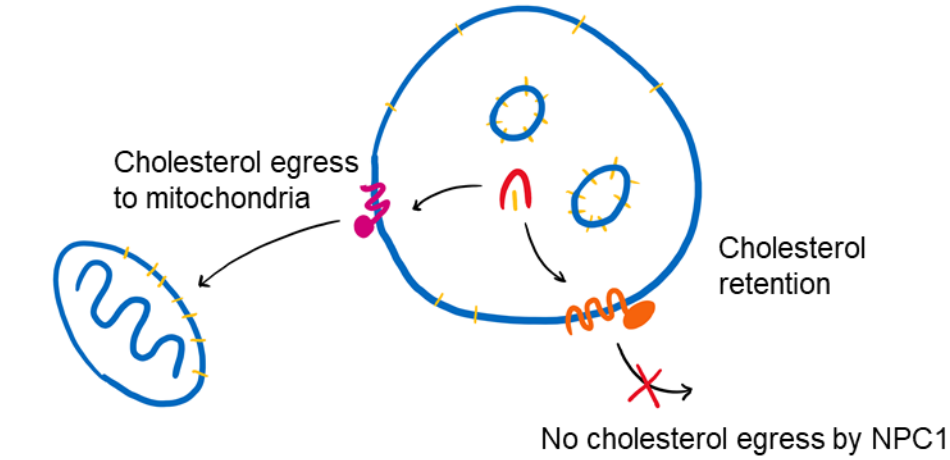

Dysfunctional NPC2

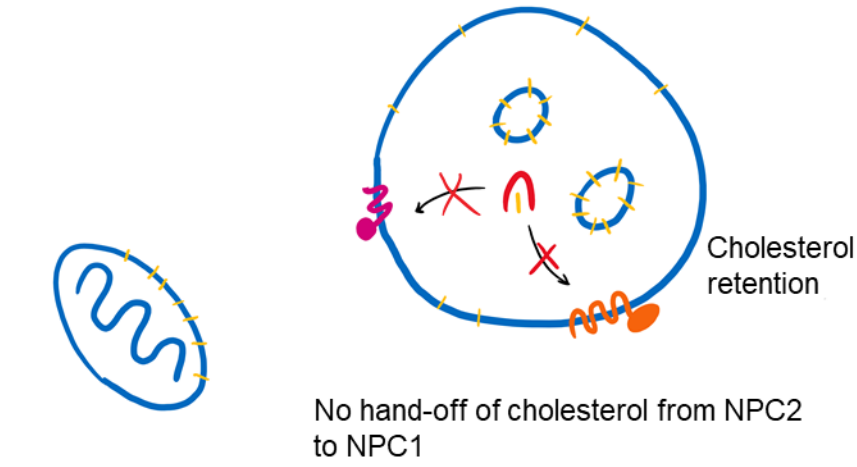

Figure 1.02 **Cholesterol Trafficking in NPC Disease**
Depiction of cholesterol trafficking from late endosomes/lysosomes. A) With functional NPC1 and NPC2, cholesterol is moved from the lumen to NPC1 via NPC2. NPC1 mediates cholesterol trafficking to the plasma membrane and ER. B) If NPC1 is dysfunctional/depleted, cholesterol accumulates in late endosomes/lysosomes, some cholesterol is transported out via NPC2 and STARD3 to the mitochondria. C) If NPC2 is dysfunctional, cholesterol is not delivered to NPC1 and accumulates in late endosomes/lysosomes. Trafficking of cholesterol to mitochondria is also disrupted.

NPC1-depleted CHO cells display increased lactate production over control cells or NPC1/STARD3 co-depleted cells (Kennedy et al., 2014). Increased lactate production indicates a shift towards a more glycolytic phenotype. Lactate levels were also found to be increased in the brain of NPC1 null mice at 3, 5 and 7 weeks of age (Kennedy et al., 2013). Increased lactate production in NPC1-depleted cells is due to mitochondrial cholesterol, as it is prevented by co-depletion of STARD3, similarly to ROS increase.

1.3.2 Connections Between Mitochondrial Cholesterol and Cancer

Many cancer cell types have elevated cholesterol compared to the normal surrounding tissues, but it is not known what role cholesterol plays in cancer cell survival (Smith and Land, 2012). Inhibition of cholesterol synthesis at HMCGR by statins reduces risk of several cancer types, including melanoma, lymphoma and breast cancers (Jacobs et al., 2011, Murtola et al., 2014, Cardwell et al., 2014). Hepatomas were found to have elevated mitochondrial cholesterol content as well, not just total cellular cholesterol (Grain, Clark and Harvey, 1983). Overexpression of STARD1 is described in some cancer as a prognostic factor (Laurich et al., 2005, Houk et al., 2004), which may also account for increased mitochondrial cholesterol. Mitochondrial cholesterol is also implicated in altering mitochondrial function in cancer cells, as increased mitochondrial cholesterol reduces mitochondrial proton leak (Baggetto, Glottes and Vial, 1992).

Studies on cultured cells have shown that cancer cell lines have increased susceptibility to apoptosis when treated with a statin, lowering cellular cholesterol production (Werner et al., 2004, Cafforio et al., 2005). Montero et al. (2008) explored the role of mitochondrial cholesterol in cancer cell susceptibility to apoptosis by chemotherapeutic drugs. Initially, they found that the hepatic cancer lines HepG2 and H35 and human hepatocellular carcinoma had elevated mitochondrial cholesterol content. Lovastatin treatment to inhibit HMG-CoA reductase and reduce cholesterol synthesis made H35 cells were more sensitive to death by several drugs, including thapsigargin, arsenic trioxide, and doxorubicin, a chemotherapeutic drug (Montero et al., 2008). Knockdown of STARD1 reduced mitochondrial cholesterol in both H35 and HepG2 cells and increased susceptibility to apoptosis for both cell lines to doxorubicin, thapsigargin and ionidamine (Montero et al., 2008), demonstrating that mitochondrial cholesterol has a role in the apoptosis resistance of some cancer cells.

1.4 The Voltage-Dependent Anion Channel

1.4.1 VDACs

Voltage-Dependent Anion Channels (VDACs) are pore-forming proteins in the outer mitochondrial membrane of all mitochondria (Kleene et al., 1987, Kayser et al., 1989, Mihara and Sato, 1985, Colombini, 1979, Colombini, 1989). Mammals have three VDAC isoforms, namely VDAC1, VDAC2 and VDAC3, of which VDAC1 is the most abundant and also the most abundant mitochondrial outer membrane protein (Messina et al., 2012). All three VDAC isoforms form β-barrel pores in the

outer mitochondrial membrane and selectively allow passage of metabolites and ions through the outer mitochondrial membrane (Magri, Reina and De Pinto, 2018). VDAC1 is composed of 19 β-strands forming a membrane-spanning pore in the outer mitochondrial membrane (Magri, Reina and De Pinto, 2018). An alpha helix resides in the center of the 2.5 nm pore when in the closed state, restricting molecule passage (Colombini, 1980). In the open state, the pore is selective, allowing passage of ATP, ADP, Ca^{2+}, and other small molecules (Colombini, 1980). VDAC exists as a monomer and in multiple oligomeric states but is most commonly dimerized (Bayrhuber et al. 2008, Ujwal et al., 2008). The influence of dimerization on the activity of VDAC is unknown, but higher-order oligomerization is linked to apoptosis (Keinan, Tyomkin, Shoshan-Barmatz, 2010).

1.4.2 VDAC1 Protein Associations

VDAC1 can oligomerize and/or form dynamic heterocomplexes with numerous cytosolic and mitochondrial proteins. Oligomerization of VDAC occurs during apoptosis induction, possibly forming a larger pore for the release of cytochrome C (Keinan et al., 2010). Apoptosis is controlled in part by the binding of pro or anti-apoptotic proteins to VDAC1. The pro-apoptotic protein BCL-2-associated X protein (BAX) induces pore formation and cytochrome C release. BAX binding to VDAC is prevented by the binding of anti-apoptotic proteins BCL-2 (B-cell lymphoma 2) or BCL-XL (B-cell lymphoma-extra-large), or by the binding of Hexokinase 1 (HXK1) (Arbel, Ben-Hail and Shoshan-Barmatz, 2012).

The association between VDAC1 and kinases including HXK1 and creatine kinase forms a direct channel for ATP/ADP exchange between these kinases and the mitochondria (Vander Heiden et al., 2010). VDAC1 also interacts with the adenine nucleotide transporter of the inner mitochondrial membrane, continuing this ATP/ADP flow directly between the mitochondrial matrix and HXK and creatine kinase (Dolder, Wendt and Wallimann, 2011). Tubulin has also been described to be a VDAC1 interacting protein and can disrupt ATP exchange by insertion within the VDAC1 ion exchange pore (Gurnev, Rostovtseva and Bezrukov, 2011).

Mitophagy, the process of recycling mitochondria, is controlled in part by the protein PINK1, which binds to VDAC (Narendra and Youle, 2011).

In polarized mitochondria, PINK1 is rapidly processed upon import, the N-terminus of the 63 kDa full length protein is cleaved by mitochondrial processing peptidase to a 60 kDa form (Green et al., 2012). The 60 kDa form of PINK1 is then cleaved again at the N-terminus by presenilin-associated rhomboid-like protease to a mature 52 kDa form (Greene et al., 2012). The mature form of PINK1 is polyubiquitinated and degraded (Deas et al., 2011, Liu et al., 2017). Proteolytic processing of PINK1 by PARL is inhibited in depolarized mitochondria, PINK1 is not ubiquitinated and remains bound to the outer mitochondrial membrane (Springer and Kahle, 2011, Lin et al., 2017, Lin and Beal, 2006). PINK1 recruits the E3 ubiquitin ligase PARKIN, which mediates the ubiquitination of mitochondrial proteins, including VDAC1 itself. (Narendra et al., 2008, Matsuda et al., 2010). PARKIN-mediated ubiquitination serves as the signal for defective mitochondria to undergo mitophagy (Matsuda et

al., 2010). Mutations in PINK1 and PARKIN have been described as causative for Parkinson's disease, due to dysregulation of mitophagy (Sun et al., 2012).

1.4.5 VDAC and Cholesterol

VDAC1 binds cholesterol (De Pinto, Benz and Palmieri, 1989, Hillier et al., 2008, Hulce et al., 2013) and other lipids, including cardiolipin and phosphatidylethanolamine, which alter VDAC channel activity and oligomerization (Rostovtseva et al., 2006 Betaneli, Petrov and Schwille, 2012). Computational mapping and photoaffinity labelling studies have identified the cholesterol binding pocket on the outer edge of the β-barrel, overlapping with a glutamate residue involved in both oligomerization and hexokinase binding (Weiser et al., 2014, Budelier et al., 2017). VDAC is part of the STARD1-containing mitochondrial protein complex thought to mediate the import of cholesterol to the inner mitochondrial membrane (Rone et al., 2012). Several studies have proposed a role for VDAC-bound cholesterol in the metabolism of cancer cells and the process of neurodegeneration, by altering its associations with binding partners (Campbell and Chan, 2008, Magri, Reina and De Pinto, 2018). In cancers, increased cholesterol in the mitochondria may alter VDAC and apoptotic protein interactions or reduce oxidative phosphorylation, contributing to the Warburg effect (Campbell and Chan, 2008). Currently, it is not known whether cholesterol does influence the protein associations of VDAC1, or what effects this would have.

1.5 Research Objectives

1.5.1 Research Aims

Aim 1: To develop a model of increased mitochondrial cholesterol, independent of disease models.

Aim 2: To explore the protein associations of VDAC under conditions of increased mitochondrial cholesterol, using the model developed in aim 1.

1.5.2 Rationale

Currently, elevated mitochondrial cholesterol is explored in the context of disease models, like NPC1. Using these models, one cannot determine what effects arise due to mitochondrial cholesterol specifically, or due to other disease processes. By developing a model of increased mitochondrial cholesterol that does not have the confounding effects of disease, we can explore effects arising from mitochondrial cholesterol and determine its impact in disease. Mitochondrial cholesterol may contribute to mitochondrial dysfunction in NPC1 (Kennedy et al., 2014), and increase the resistance of some cancer cells to apoptosis (Montero et al., 2008). Due to the highly varied associations of VDAC and cholesterol-binding properties, cholesterol could modulate VDAC associations and downstream cellular processes, including metabolism, apoptosis, and ER-mitochondria contact sites. The role of cholesterol in VDAC complex formation and whether it has a connection to disease pathogenesis is unknown.

I hypothesize that cholesterol content of the outer mitochondrial membrane influences the binding of VDAC1 to other proteins, altering metabolism and other processes.

CHAPTER 2: MATERIALS AND METHODS

2.1 Cell Models

2.1.1 SH-SY5Y, HEK and CHO Cell Culture

Human neuroblastoma SH-SY5Y cells obtained from American Type Culture Collection (ATCC, cat. no. CRL-2266) were maintained in 50% Dulbecco's modified eagles medium (DMEM) (Life Technologies, Carlsbad, CA, cat. no. 12800017), 50% Ham's F12 (Life Technologies, cat. no. 21700-075) supplemented with 5% FBS (Fetal bovine serum) (Wisent Bioproducts, Saint-Jean-Baptiste, QC) and 5% NuSerum cell culture supplement (Fisher Scientific) in a humidified atmosphere (5% CO_2, 37°C). Human embryonic kidney 293T (HEK) cells were maintained in DMEM supplemented with 10% FBS in a humidified atmosphere (5% CO_2, 37°C). SH-SY5Y and HEK cells were subcultured every 4 days at a split ratio of 1:4 and 1:8, respectively. Chinese hamster ovary (CHO) cells were maintained in Ham's F12 supplemented with 5% FBS in a humidified atmosphere (5% CO_2, 37°C) and subcultured every 3 days at a 1:8 split ratio.

2.2 Molecular Biology

2.2.1 Vectors

Generation of pLenti OMM YFP FKBP-12 rapamycin binding domain (FRB) P2A mCherry FK506-binding protein (FKBP) StARD4 vectors (Appendix A): Cassettes of OMM-YFP-FRB and OMM-YFP with C-terminal addition of a P2A element were

created by PCR amplification using eYFP Mitotrap (Addgene # 46942) as a template and primers (Table 2.1). Cassettes of mCherry-FKBP-StARD4 with a N-terminal addition of a P2A element were created by PCR amplification of pcDNA3.1(+) zeo mCherry-FKBP-StARD4 or pcDNA3.1(+) zeo mCherry-StARD4. Gibson assembly (New England Biotech) was used to join PCR amplicons with AgeI, MluI digested pLenti MP2 (Addgene # 36097) backbone.

Generation of pLenti OMM GlySer V5 StARD4 P2A Clover and pLenti OMM GlySer V5 StARD4$_{W108D}$ P2A Clover (Appendix A): OMM was amplified by PCR using EYFP Mitotrap as a template and primers (Table 2.1). The V5 epitope with a 5' glycine-serine linker was amplified by PCR using pLenti Syn DHCR24 link V5-APEX2 as a template and primers (Table 2.1). StARD4 was amplified by PCR using *pLenti OMM YFP FRB P2A mCherry FKBP StARD4* as a template and primers (Table 2.1). StARD4 with a point mutation to create the W108D mutant was created in two separate PCR reactions to amplify the 5' and 3' ends separately, with primer overlaps containing the point mutation. P2A-clover was PCR amplified using pLenti Syn Ruby3 P2A Cloveractin VAPAmG as a template and primers (Table 2.1). Gibson assembly was used to join PCR amplicons into AgeI, MluI digested pLenti MP2 backbone.

Generation of px459 sgCHO-VDAC1: px459 plasmid (Addgene # 62988) was digested with BbsI (New England Biolabs), and a single-strand DNA oligonucleotide (Table 2.1) was incorporated, containing a sequence encoding the sgRNA targeting VDAC1 and overlaps with the px459, via Gibson assembly.

Table 2.1 Primers

Oligonucleotide	*Sequence*
Cloning	
pLenti CMV OMM YFP FRB P2A mCherry FKBP STARD4 plasmids	
OMM-FRB-YFP F	CATCCACGCTGTTTTGACCTCCATAGAAGACACCGCCCGGGTTC GCCACCATGAAGAGCTTCATTACAAGGAACAAGAC
OMM-FRB-YFP R	GGGTTCTCCTCCACGTCTCCAGCCTGCTTCAGCAGGCTGAAGTT AGTAGCTCCGCTTCCCGTACGGTGCGGAGCCTGCGTAGTCG
OMM-FRB F	CATCCACGCTGTTTTGACCTCCATAGAAGACACCGCCCGGGTTC GCCACCATGAAGAGCTTCATTACAAGGAACAAGAC
OMM-FRB R	GGTTCTCCTCCACGTCTCCAGCCTGCTTCAGCAGGCTGAAGTTA GTAGCTCCGCTTCCCGTACGGCCGGCCTGCTTTGAGATTCG
mCherry-FKBP-STARD4 / mCherry-STARD4 F	AGCGGAGCTACTAACTTCAGCCTGCTGAAGCAGGCTGGAGACGT GGAGGAGAACCCTGGACCTATGGTGAGCAAGGGCGAGGAG
mCherry-FKBP-STARD4 / mCherry-STARD4 R	GTCTAGAACGCGTGAATTCACTAGTATGCATCTCGAGCACCGGT TCATAAAGCTTTTCGTAAATCACCATAGAAGTTGG
pLenti CMV OMM linker V5 STARD4 P2A Clover plasmids	
OMM F	GCGTACGGGATCCCACCGGTGCCACCATGGTGGGCCGGAACAG
OMM R	ACCTCCGGATCCACCACCACCAGAACCACCTCC
V5 F	GGTGGTTCTGGTGGTGGTGGATCCGGAGGTTCAG
V5 R	AGACAGGCCTTCCATGGTGCTGTCCAGGCCC
STARD4 F	GGCCTGGACAGCACCATGGAAGGCCTGTCTGATGTT
STARD4 R	AAGTTTGTTGCTCCGGATCCTAAAGCTTTTCGTAAATCACCATA GAAGT
Clover F	ACTTCTATGGTGATTTACGAAAAGCTTTAGGATCCGGAGCAACA AACTT
Clover R	CCTGCAGGTCTAGAACGCGTTTACTTGTACAGCTCGTCCATGC
CRISPR	
Homology 1 F	TCCCCGACCTGCAGCCCAGCTGAGGTGTGACACTTATTTCCAGG
Homology 1 R	CCGGAACCTCCTCCGCTCCCTGCTTGAAATTCCAGTCCGAGACC
Homology 2 F	AGTTCTTCTGATTCGAACATCGTACAATCGTTAATTTTAAACT ATTTTGCAG
Homology 2 R	TGGAGAGGACTTTCCAAGGAGGTCACTTTAAATCCCTAGTGTTG TC
px459 sg insert	TATATATCTTGTGGAAAGGACGAAAGGGTGGCCACAAGCTTGGT CTGTTTTAGAGCTAGAAATAGCAAGTT
CRISPR screening	
Screen F	GCTGTTTTCTTCCATCCTTTTCC
Screen R	CACAAAATGGAAGACTCTATAATGTATCC
qPCR	
Ppia qPCR Forward	TCTTCTTGCTGGTCTTGCCATTCC
*Ppia q*PCR Reverse	TCCAAAGACAGCAGAAAACTTTCG
Nfe2l2 qPCR Forward	GCTTCTTTCCATTCCCGAATTAC
Nfe2l2 qPCR Reverse	TGAGCTGGCTGGCGTCTTC

Generation of pFETCh CHO-VDAC1: Homology arms of approximately 700 bp flanking the stop codon of the CHO VDAC1 gene were produced by PCR using CHO genomic DNA as a template and primers (Table 2.1). The homology arm amplicons were incorporated into BsaI, BbsI digested pFETCh_donor plasmid (Addgene # 63934).

2.2.2 Lentivirus Production

Lentiviruses were produced using the pLenti transfer plasmids described above. HEK cells were plated the day before transfection for 50% confluency at the time of transfection. For the transfection of one 10 cm diameter dish, the transfer plasmid (5.8 μg), envelope plasmid (pMD2.G, Addgene #12259, 1.2 μg), and packaging plasmid (psPAX2, addgene #12260, 3 μg) were incubated for 20 minutes in 1 mL minimal essential medium with 40 μg/mL polyethyleneimine. The DNA mixture was added to 7 mL DMEM (5% FBS) on 50% confluent HEK-293T cells and incubated for 5 hours. After 5 hours, medium was changed to DMEM (10% FBS). Virus containing medium was harvested 48 hours post-infection and debris removed by centrifugation at 800 g followed by filtration through a 0.45-micron syringe filter. Virus-containing medium was concentrated 50x using a Macrosep 100,000 kDa molecular weight cutoff filter (PALL Biosciences) at 2000 g.

2.2.3 Lentivirus Transduction

Mammalian cells at 50% confluency were transduced with concentrated virus-containing medium at varying dilutions, which were adjusted to achieve 90%

transduction efficiency, determined by the number of fluorescent cells. Transduced cells were seeded into culture plates 48 hours post-infection for experiments.

2.2.4 RT-qPCR

Total mRNA was isolated from single wells of 6-well plates of CHO cells using an EZ-10 RNA miniprep kit (Bio Basic, Markham, ON), according to manufacturer instructions. iScript reverse transcriptase (BioRad) was used to prepare 1 μg cDNA, according to manufacturer instructions.

Quantitative PCR (qPCR) was performed with 60 ng cDNA using iSYBR Green Mastermix (BioRad), according to manufacturer instructions in an Eppendorf Realplex instrument. A template dilution curve was used to determine primer pair efficiency. Primers used for qPCR analysis are listed in Table 2.1. Melting curve analysis was performed after qPCR to verify specificity of the primers for one target. The Pfaffl method was used to calculate relative abundance of the target genes, with *Ppia* used as a reference gene.

2.2.5 DNA Isolation

CHO cells grown in 96-well cell culture plates were used for genomic DNA isolation. Cells from one well were dissociated by trypsinization and resuspended in 200 μL phosphate-buffered saline (PBS). Trypsin was removed by pelleting the cells at 800 g and resuspending in 20 μL 5 mM Tris (pH 8.5). The cells were heated for 15 min at 99°C to lyse and cooled on ice before pelleting unbroken cells at 800 g. Five

microliters of the resulting supernatant, containing genomic DNA, was used undiluted as a template for PCR.

2.3 CRISPR

2.3.1 CRISPR Knock-in

A CRISPR knock-in edited cell line was created with a 3X FLAG epitope tag fused to VDAC1 using the pFETCH method (Savic et al., 2015) (Figure 2.01). Briefly, 9 µg px459 sgCHO-VDAC1 and 3 µg pFETCH CHO-VDAC1 were incubated with 40 µg PEI in 1 mL MEM. The DNA mixture was added to 50% confluent CHO cells in 7 mL Ham's F12 (2.5% FBS) and incubated in a humidified atmosphere (5% CO_2, 37°C) for 6 hours. After incubation, cell culture medium was exchanged for Ham's F12 (5% FBS). At 48 h post-transfection, medium was replaced with Ham's F12 (5% FBS) supplemented with 5 µg/mL puromycin for the selection of px459 sgCHO-VDAC1 transfected cells. At 72 h post-transfection, medium was replaced with Ham's F12 (5% FBS) supplemented with 100 µg/mL G418 and 2 µM ganciclovir for the selection of CRISPR edited cells, and selection against incorporation of the pFETCH CHO-VDAC1 plasmid. The cells were re-seeded at 50,000 cells per 10 cm dish and Ham's F12 (5% FBS) supplemented with 100 µg/mL G418 was replaced every two days until single colonies were visible by eye. Single colonies were isolated by trypsinization using cloning rings and maintained as individual monoclonal cell lines.

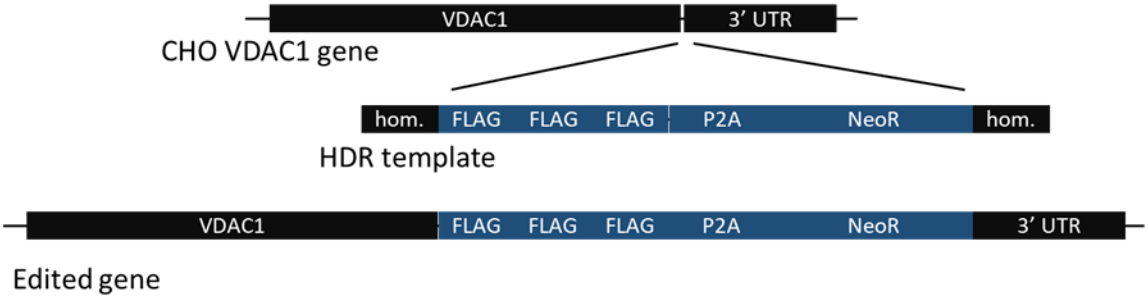
VDAC1
3' UTR
CHO VDAC1 gene
hom.
FLAG
FLAG
FLAG
P2A
NeoR
hom.
HDR template
VDAC1
FLAG
FLAG
FLAG
P2A
NeoR
3' UTR
Edited gene

Figure 2.01 **pFETCH CRISPR Knock-in Layout**
Depiction of wildtype CHO VDAC1, homology-directed repair template and resulting knock-in edited VDAC1 gene layout.

2.3.3 Screening

Monoclonal cell lines were screened by PCR amplification of the end of VDAC1 from cDNA using primers (Table 2.1). Screening amplicons were sequenced (Eurofins Genomics, Toronto, ON) and compared to the theoretical sequences using ApE plasmid editing software.

2.4 Cellular Assays

2.4.1 Lactate Production Assay

Cells for lactate production assay were plated at 50,000 cells per well of a 24-well tissue culture plate. After 48 h, cells were washed once with PBS and incubated in lactate efflux medium (Phenol-red, serum, and glucose-free DMEM) supplemented with 10 mM glucose for 4 h. Lactate efflux medium was centrifuged at 10,000 g to remove cellular debris. Cells were lysed in 0.3 M NaOH with shaking for 1 h at room temperature. Ten microliters of sample efflux medium or lactate standards (1000, 500, 250, 125, 62.5, 31.25, and 0 μM L-lactate in water (Sigma L7022)) were incubated in lactate assay buffer (75 mM Tris HCl, 100 mM KCl, 0.0004% Triton X-100) with 1 mM β-NAD^+, 4.8 μM resazurin, 1 U/mL diaphorase and 18.5 U/mL L-lactate dehydrogenase for 30 minutes at room temperature. Resorufin is produced in a 1:1 ratio to lactate present in the sample, resorufin was measured fluorometrically with an excitation filter of 540 nm and emission filter of 590 nm in a FLUOstar Optima plate reader (BMG Labtech). Lactate production was standardized to protein content of the wells, determined with a BCA assay

performed according to manufacturer instructions (Thermo Fisher). Triplicate measurements were taken of triplicate wells of three independent experiments.

2.4.2 Mitochondrial Cholesterol Import Assay

Stably transfected CHO cells expressing the F2 fusion protein (Huang and Miller, 2001, Kennedy et al., 2017) were plated into 48-well plates for mitochondrial cholesterol import, the cells were washed once with PBS and medium was changed to 300 µL import medium (phenol-red free, serum free DMEM with 10 µM trilostane (Steraloids, Newport, RI)). To determine maximal pregnenolone production, 5 µM 22R-hydroxycholesterol (Steraloids) was supplemented to the pregnenolone assay medium. After 24 hours, import medium was harvested and cells were lysed for protein assay with 0.3 M NaOH, shaking 1 h at room temperature.

Pregnenolone produced by F2 CHO cells was assayed by radioimmunoassay as previously described (Kennedy et al., 2017)). Briefly, 50-100 µL of samples were incubated with anti-pregnenolone antibody (1:810) (MP Biomedicals #07172016), and ^{3}H-radiolabeled pregnenolone ([7-^{3}H(N)]pregnenolone, 11.5 Ci/mmol) (Perkin-Elmer, Waltham, MA), 166.6 bq) in 700 µL phosphate buffer (60 mM sodium phosphate dibasic, 40 mM sodium phosphate monobasic pH 7.0, 155 mM sodium azide, 155 mM sodium chloride, 0.2% gelatin) for 18 h at 4°C. 200 µL dextran-coated charcoal (6.88 mg/mL) in phosphate buffer without gelatin was added to each reaction for 30 minutes. Charcoal was pelleted via centrifugation and the supernatants were each added to 4 mL of EcoLite scintillation cocktail (VWR) in scintillation vial, briefly vortexed, and radioactivity was measured by scintillation

counting. Each assay included a pregnenolone standard curve in duplicate (0 – 500 pg pregnenolone (Sigma), a total count control excluding antibody and charcoal, as well as a non-specific binding control that excluded only the antibody. Triplicate measurements were taken of triplicate wells of three independent experiments and standardized to protein content.

2.4.3 Mitochondria Isolation

Cells from 12 10 cm diameter tissue culture dishes were harvested into mitochondria isolation buffer (MIB) (5 mM Hepes, pH 7.4, 250 mM mannitol, 1 mM EGTA, 70 mM sucrose) with PMSF (1 mM), leupeptin (100 μM), pepstatin (1 μM) and aprotinin (2 μg/mL). The cells were lysed by nitrogen cavitation in a PARR 4639 vessel (PARR Instruments, Moline, IL) at 1500 PSI for 7 minutes on ice. Nuclei and unbroken cells were removed by centrifugation at 800 g for 10 minutes at 4°C. Crude mitochondria and lysosomes were pelleted from nuclei-free lysate by centrifugation at 10,000 g for 15 minutes at 4°C. For crude mitochondria samples, the crude mitochondria were resuspended in MIB and centrifuged again to remove cytosolic proteins. The supernatant was also centrifuged again to remove residual mitochondria and lysosomes. To obtain further purified mitochondria, the crude mitochondria were resuspended and layered on top of a 10/23/50% gradient of Percoll (Sigma) in MIB. The gradients were centrifuged at 35,000 g for 20 minutes in an SW60Ti Rotor (Beckman Coulter, Brea, CA). Mitochondria settle at the 23/50% interface, while endosomes and lysosomes are more predominant at the 10/23% interface. The material at both interfaces was collected and diluted 30 x in MIB.

Mitochondria and lysosomal fractions were recovered by centrifugation at 16,000 g and resuspended 120 µL in 1x PBS with 0.1% sodium dodecyl sulfate (SDS).

2.4.4 Cholesterol Assay

Cholesterol content in isolated mitochondria was determined by enzymatic assay using Amplex Red as described previously (Amundson and Zhou, 1999). Briefly, mitochondria samples or cholesterol standards were incubated with Amplex Red (Sigma) (37.5 µg/mL), horseradish peroxidase (HRP) (Sigma) (1 U/mL), and cholesterol oxidase (Sigma) (1 U/mL) in cholesterol reaction buffer (0.1 M potassium phosphate pH 7.4, 0.05 M NaCl, 0.1% TritonX-100) for 15 minutes at 37°C. Cholesterol oxidase produces H_2O_2 as it oxidizes cholesterol to cholest-4-ene-3-one; HRP catalyzes the conversion of amplex red to the fluorescent molecule resorufin in the presence of H_2O_2. Resorufin fluorescence is measured with 750 nm excitation and 590 nm emission filters in a FLUOstar Optima plate reader. Cholesterol was measured in triplicate.

2.5 Microscopy

2.5.1 Immunostaining and Filipin Stain

Cells grown on glass coverslips were fixed with 3% (w/v) paraformaldehyde for 15 min, then permeabilized with 0.1% Triton X-100 for 10 min, and blocked in blocking solution (5% goat serum, 2% BSA in PBS) for 30 min. Primary antibodies (Table 2.2) were diluted in blocking solution, and incubated on coverslips overnight at 4°C. Secondary antibodies conjugated to fluorophores were diluted in blocking

solution and incubated on coverslips for 2 h at room temperature. Coverslips were mounted in AquaMount mounting solution (Thermo Fisher Scientific). Filipin staining was performed without Triton X-100 permeabilization, 50 μg/mL Filipin III complex (Sigma) was added to the blocking and antibody solutions.

2.5.3 Image Acquisition and Analysis

Images of immunostained and filipin stained cells were acquired using a Nikon TE2000 epifluorescence microscope equipped with a CCD camera and a 60x oil immersion objective with a numerical aperture of 1.4. Microscopy images are representative of 5 images taken of each coverslip, produced in triplicate in three independent experiments. Background subtraction was performed with FIJI image analysis software (Schindelin et al., 2012) using the rolling ball algorithm.

2.6 Protein Assays

2.6.1 Immunoblotting

Generation of cell lysates: Mammalian cells grown in a monolayer were washed once with cold PBS, then scraped into cold radioimmunoprecipitation assay (RIPA) buffer (20 mM Tris-HCl, 150 mM NaCl, 1 mM EDTA,1 % NP-40, pH 7.5) with 0.1% SDS. Scraped cells were incubated 20 minutes on ice, then homogenized with 5 gentle passes through a 21-gauge needle. Homogenized lysate was centrifuged at 15,000 x g and 4°C for 15 m, and the supernatant was recovered.

Samples for immunoblotting were separated via SDS-PAGE on a 12% polyacrylamide gel at 100 V. Proteins were transferred to 0.2-micron nitrocellulose

membranes (Life Technologies) overnight at 30 V or for 1 hour at 100 V. Protein transfer was verified using Pierce reversible protein stain (Thermo Scientific) according to manufacturer instructions. Membranes were blocked with 5% milk in tris-buffered saline with tween20 (TTBS) for one hour, prior to probing overnight at 4°C with primary antibodies (Table 2.2) in 2% BSA in TTBS. Secondary antibodies conjugated to horseradish peroxidase (Jackson Immunoresearch, West Grove, PA) against rabbit, goat or mouse were prepared at a dilution of 1:10,000 in 5% milk in TTBS and incubated on membranes for 2 hours at RT. Enhanced chemiluminescence (BioRad) was used for the detection of HRP with a VersaDoc MP4000 (BioRad) imager or X-ray film (Santa Cruz Biotechnology, Dallas, TX).

2.7 Statistical Analysis

Data for all experiments was interpreted using Microsoft Excel (2016), figures were produced, and statistical analysis was performed using GraphPad Prism version 8.0 (GraphPad Software, La Jolla, CA). Comparisons of two groups was performed using an unpaired T-test, while more than two groups were compared using a one-way ANOVA with Tukey's multiple comparison post-test. Differences were assumed to be significant if $P<0.05$.

CHAPTER 3: RESULTS

3.1 Acute Model of Elevated Mitochondrial Cholesterol

3.1.1 Chemically Induced Translocation of STARD4 to Mitochondria

Chemically induced translocation (CIT) can be used to acutely sequester proteins away from their area of activity using two different rapamycin binding domains, FRB and FKBP, and rapamycin to induce heterodimerization (Robinson et al., 2010). A previous study exploring the role of STARD4 in cholesterol transport between the plasma membrane and the ERC used CIT to sequester STARD4 to the mitochondria, incidentally finding potentially elevated mitochondrial cholesterol (Iaea et al., 2017). I began using this system to investigate the consequences of acute elevations of mitochondrial cholesterol in relation to metabolism and disease in SH-SY5Y neuroblastoma cells.

In the construct pLenti_OMM-YFP-FRB_P2A_mCherry-FKBP-STARD4, the FRB domain was fused to an N-terminal outer mitochondrial membrane targeting sequence (OMM) with YFP in the middle (OMM+FRB), while the FKBP domain was fused N-terminally to STARD4, with mCherry fused to the FKBP domain (STARD4+FKBP). Addition of rapamycin would induce heterodimerization of FRB and FKBP, translocating STARD4 to the outer mitochondrial membrane (STARD4-CIT) (Figure 3.01 A). Two variants were produced of OMM YFP and mCherry STARD4 without FRB or FKBP domain (OMM-FRB and STARD4-FKBP) and used as negative controls for CIT of STARD4 to mitochondria. The constructs missing either

binding domain were used to control for any effects arising from the presence of the binding domains.

Addition of rapamycin to STARD4-CIT expressing cells with StARD4+FKBP and OMM+FRB induced colocalization of STARD4+FKBP with the mitochondrial outer membrane targeted OMM-FRB (Figure 3.02 A). Cells expressing StARD4-FKBP and OMM+FRB, or StARD4+FKBP and OMM-FRB had no colocalization of STARD4-/+FKBP to OMM+/-FRB upon rapamycin treatment. Further, with both FRB and FKBP present, but no rapamycin treatment, colocalization also was not observed. Colocalization of STARD4+FKBP with OMM+FRB indicates successful translocation of STARD4 to the mitochondria. This effect was observed as early as 20 minutes after addition of rapamycin and still up to four hours, giving a four-hour window for the exploration of effects arising acutely to translocation.

The STARD4-CIT system was made using a P2A element, which is a self-cleaving peptide of the 2A peptide family (Liu et al., 2017). The P2A element allows for approximately equimolar co-expression of the two components. Immunoblotting was performed to verify expression of both proteins for STARD4-CIT with or without either FRB and FKBP (Figure 3.02 B). Anti-RFP and anti-GFP antibodies were used to probe for mCherry on the STARD4+/-FKBP fusions and YFP on the OMM+/-FRB fusions, respectively. Both protein fusions were expressed for all three constructs, with a corresponding change in kDa with or without the rapamycin binding domains. By overexposing the immunoblot image (Figure 3.02 C), high

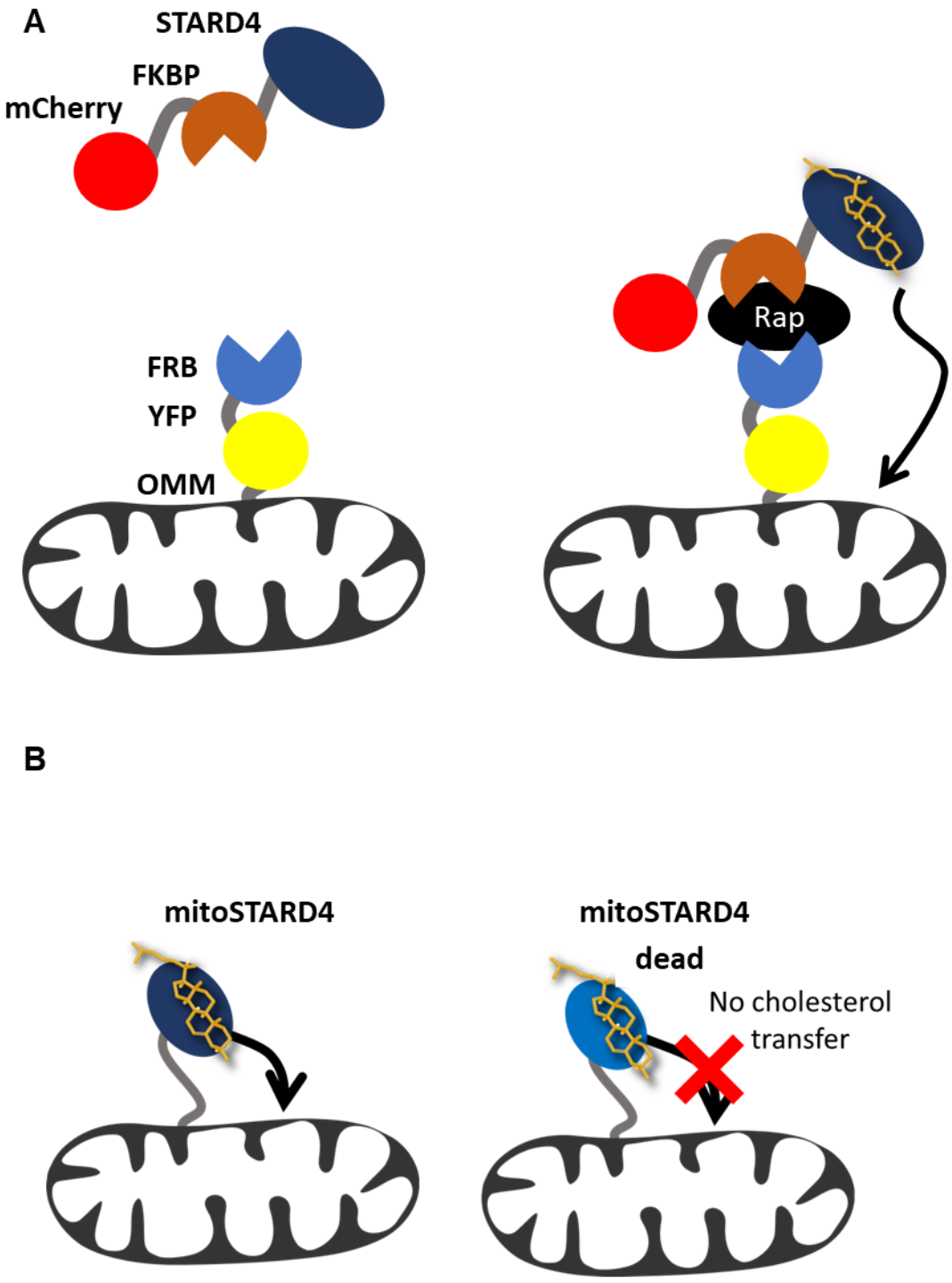
A
STARD4
FKBP
mCherry
FRB
YFP
OMM
Rap
B
mitoSTARD4
mitoSTARD4
dead
No cholesterol
transfer

Figure 3.01 **STARD4-CIT, MitoSTARD4 Models**
A) Depiction of the STARD4-CIT model; outer mitochondrial membrane targeted FRB domain-YFP fusion is expressed along with mCherry-FKBP-STARD4 fusion. Addition of rapamycin induces STARD4 translocation to mitochondria, directing cholesterol trafficking to mitochondria. B) Depiction of the MitoSTARD4 model; outer mitochondrial membrane targeted STARD4 protein directs cholesterol trafficking to mitochondria, MitoSTARD4-Dead mutant does not.

A

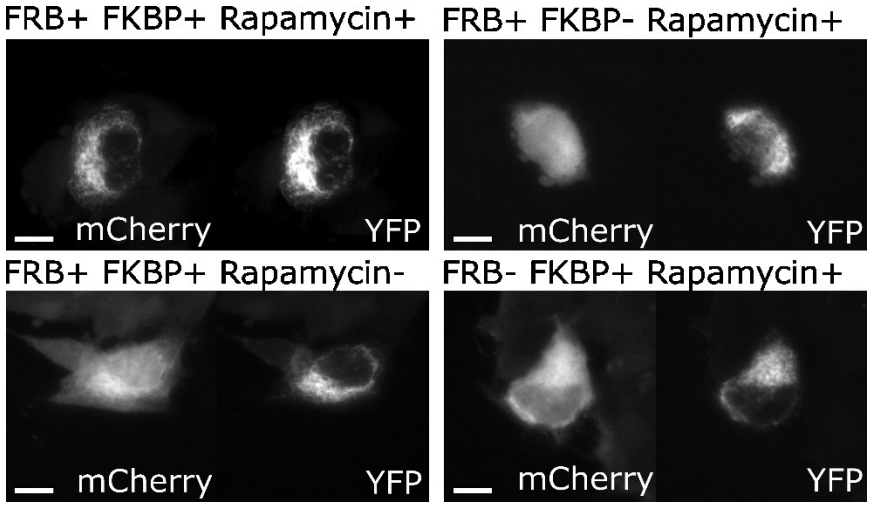
FRB+ FKBP+ Rapamycin+
mCherry
YFP
FRB+ FKBP- Rapamycin+
mCherry
YFP
FRB+ FKBP+ Rapamycin-
mCherry
YFP
FRB- FKBP+ Rapamycin+
mCherry
YFP

B

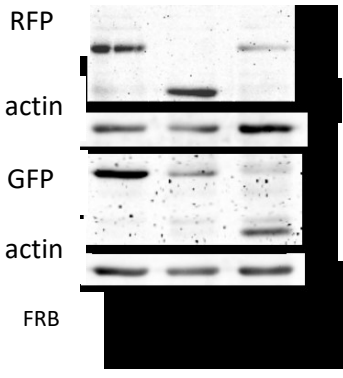
RFP
actin
GFP
actin
FRB
mCherry
mCherry
OMM YFP
OMM YFP
FRB

C

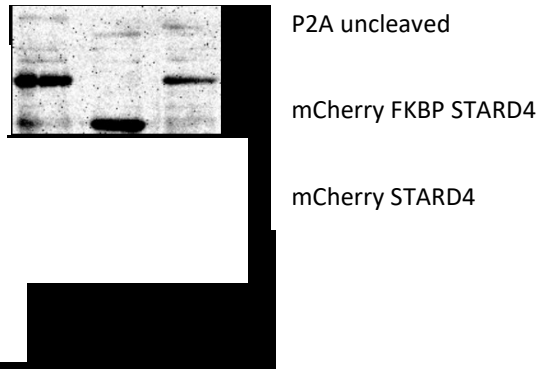
P2A uncleaved
mCherry FKBP STARD4
mCherry STARD4

Figure 3.02 **Rapamycin Treatment Induces Translocation of STARD4-FKBP to OMM-FRB**
SH-SY5Y cells transduced with STARD4-/+FKBP and OMM-/+FRB as indicated were incubated with or without 200 nM rapamycin for 4 h. A) Fluorescence microscopy of mCherry-STARD4 (mCherry) and OMM-YFP (YFP). Scale bars 10 μm. B) Immunoblot of SH-SY5Y cell lysates transduced with STARD4-CIT with and without FRB and FKBP domains probed with antibodies against RFP or GFP. Actin was used as a loading control. 10 μg protein per lane. C) Top panel from B, overexposed to show weak protein bands.

molecular weight bands were identified that correspond to protein produced by a non-functioning P2A element, not properly cleaved into two proteins.

3.1.2 Acute Translocation of STARD4 to Mitochondria does not Alter Lactate Production

Lactate production is increased in NPC1-deficient CHO cells (Kennedy et al., 2014) and brain of NPC1-null mice (Kennedy et al., 2012). I measured lactate production upon addition of rapamycin in the STARD4-CIT model, to explore whether the phenotype of increased lactate production is present in this model. Lactate was not elevated as a result of STARD4 translocation (Figure 3.03). However, lactate production was reduced when STARD4+FKBP was expressed in combination with OMM-FRB, regardless of the presence or absence of rapamycin (Figure 3.03). Rapamycin treatment did not induce changes in lactate in any of the groups (Figure 3.03). Reduction in lactate production when only the FKBP domain was present in the STARD4-CIT system suggests that expression of the FRB domain elevates lactate production, which does not occur when the domain is not present. Alternatively, FKBP expression reduces lactate production when the binding partner, FRB is not present. As there was no increased lactate production in the STARD4-CIT system with both FRB and FKBP, a 4h acute translocation of STARD4 to mitochondria may not be a long enough timeframe to induce increased lactate production, or lactate production may not be affected by acute translocation of STARD4 to mitochondria.

3.1.3 Potential Issues with Acute STARD4 Translocation

In the STARD4-CIT model, it seemed as though effects arose from the expression of one of the rapamycin-binding domains. When STARD4-FKBP was expressed without expression of an RFB domain, lactate production was decreased compared to when both domains or only FRB were present. Metabolic disturbances arising from the STARD4-CIT system itself and not from the acute translocation of STARD4 would be confounding for exploring the acute alterations to metabolism. The use of rapamycin required by STARD4-CIT is also a drawback, as rapamycin influences metabolism through inhibition of mTOR (Sabers et al., 1995, Brown et al., 1994, Lee et al., 2017), and could mask changes that might otherwise occur. The SH-SY5Y neuroblastoma cells were difficult to culture and were inconsistent in growth and possibly metabolism. I made the decision to switch from the STARD4-CIT model to a more chronic model that does not rely on rapamycin binding domains or rapamycin. SH-SY5Y cells were also left in favor of CHO cells for consistency and ease of culture. CHO cells are also a more direct comparison to previous work in NPC1-deficient CHO cells.

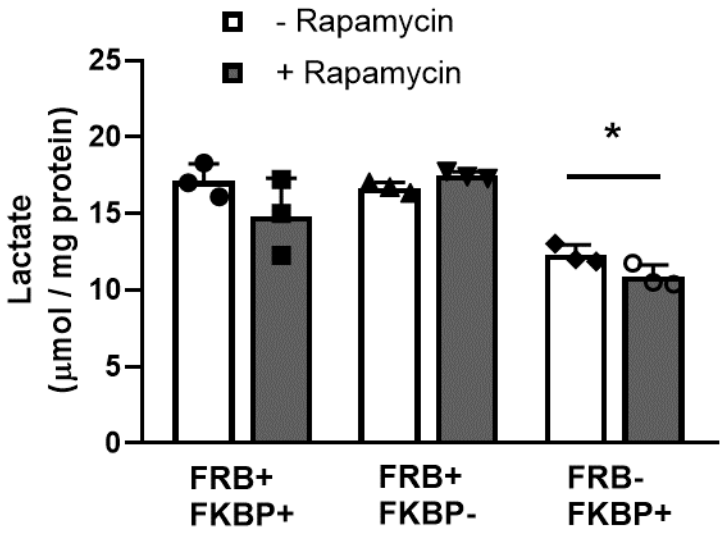
- Rapamycin
+ Rapamycin
Lactate
(µmol / mg protein)
25
20
15
10
5
0
*
FRB+
FKBP+
FRB+
FKBP-
FRB-
FKBP+

Figure 3.03 **STARD4-FKBP Acutely Translocated to Mitochondrial OMM-FRB does not Increase Lactate Production**
SH-SY5Y cells transduced with STARD4-/+FKBP and OMM-/+FRB as indicated were incubated with or without 200 nM rapamycin for 4 h. Lactate was measured in the medium collected at the end of the 4 h treatment period. Graph shows the mean ± SD of three independent experiments in triplicate.

3.2 Outer Mitochondrial Membrane-Targeted STARD4 – a Chronic Model of Elevated Mitochondrial Cholesterol

3.2.1 MitoSTARD4 Model

Forgoing the acute STARD4 translocation model, I decided to constitutively express STARD4 on the mitochondrial outer membrane (MitoSTARD4). The construct used for this, pLenti OMM GS V5 STARD4 P2A clover, consisted of an N-terminal outer mitochondrial membrane targeting sequence fused to a glycine-serine repeat linker, V5 epitope tag and STARD4. A P2A element was used for co-expression of clover as a green fluorescent reporter. This model forgoes the rapamycin binding domains and is essentially a chronic version of the acute STARD4-CIT system. The W108D mutation in human STARD4 was previously described to be deficient in cholesterol transfer activity (Iaea et al., 2015). The W108D mutant STARD4 was used in place of wildtype STARD4 (MitoSTARD4 Dead) as a control for the expression of mitochondrially targeted STARD4, as there may be effects arising from excess protein in the mitochondrial outer membrane. By creating a model of increased mitochondrial cholesterol independent of disease models, we aim to use this to determine what effects in NPC and other diseases may be arising purely due to increased mitochondrial cholesterol.

3.2.2 MitoSTARD4 Colocalizes with Mitochondrial Marker TOM20

Immunoblotting with anti-V5 antibodies showed comparable expression levels of MitoSTARD4 WT and Dead (Figure 3.04 A). Immunofluorescence was used

to verify proper mitochondrial localization of the MitoSTARD4 WT and Dead fusion proteins. The V5 tag on the fusion proteins colocalized well with TOM20, an outer mitochondrial membrane protein. (Figure 3.04 B).

3.2.3 MitoSTARD4 Expression does not Cause Overt Alterations to Cellular Cholesterol Distribution

Iaea et al. observed increased mitochondrial filipin staining upon acute translocation of STARD4 to mitochondria, concluding that there was accumulation of cholesterol in peri-mitochondrial vesicles (Iaea et al., 2017). To determine whether MitoSTARD4 induces the formation of cholesterol-enriched peri-mitochondrial vesicles, or otherwise alters cholesterol distribution, I used filipin staining to visualize the distribution of unesterified cholesterol (Figure 3.04 C). Filipin staining was similar in both MitoSTARD4 WT and MitoSTARD4 Dead, with staining throughout the cell and a bright spot in the center, likely corresponding to the endocytic recycling compartment (Mukherjee et al., 1998). Immunofluorescence against TOM20 was used concurrently with the filipin staining as a mitochondrial marker. Neither MitoSTARD4 WT or MitoSTARD4 Dead expressing cells had filipin staining that appeared to co-localize with TOM20. These findings suggest that MitoSTARD4 expression does not induce a filipin-detectable accumulation of mitochondrial cholesterol. Given the low physiological level of cholesterol in mitochondria, mitochondrial filipin staining would only have been expected if cholesterol levels rose far beyond physiological or even disease-associated levels.

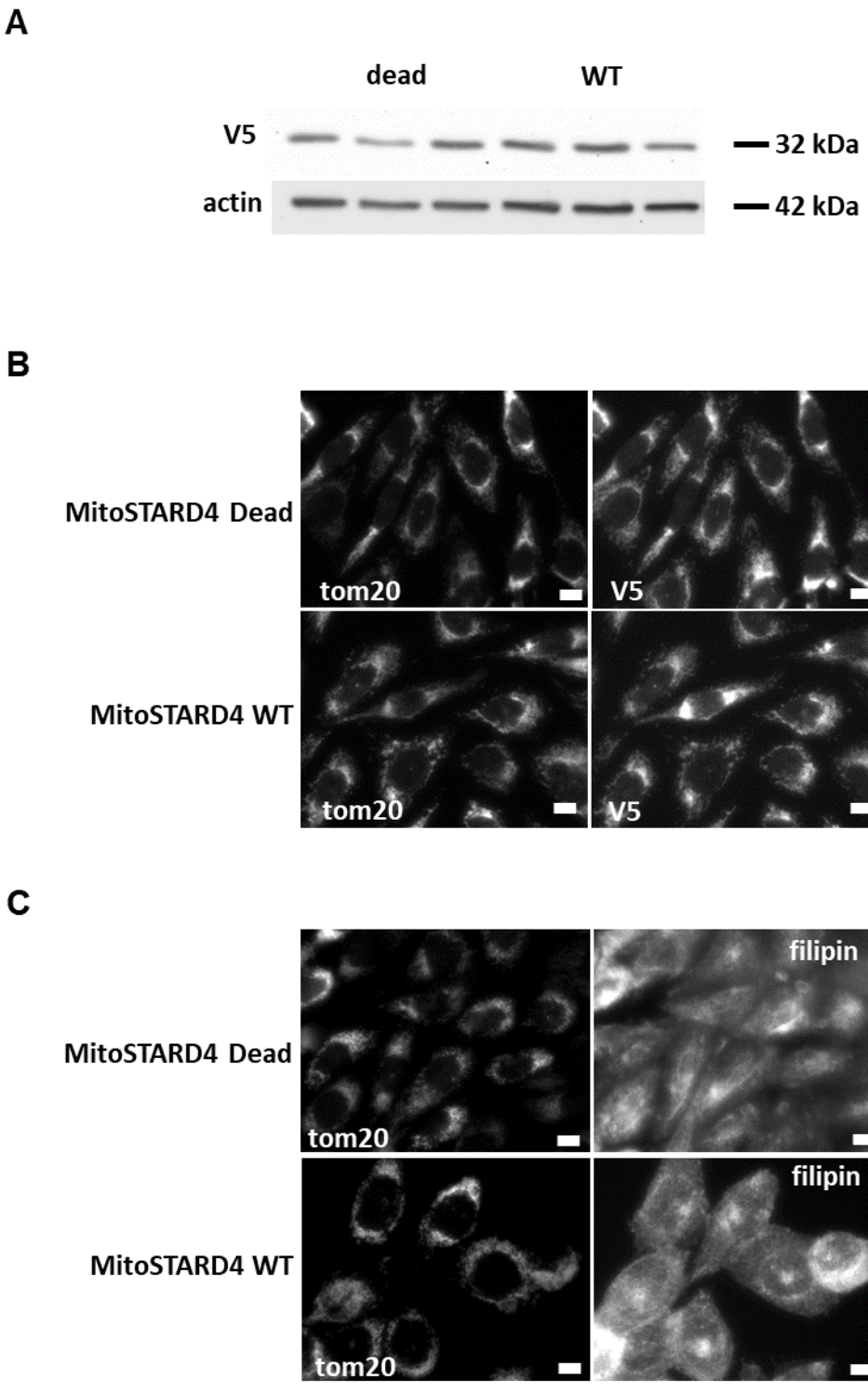
A
dead
WT
V5
32 kDa
actin
42 kDa
B
MitoSTARD4 Dead
tom20
V5
MitoSTARD4 WT
tom20
V5
C
MitoSTARD4 Dead
tom20
filipin
MitoSTARD4 WT
tom20
filipin

Figure 3.04 **MitoSTARD4 WT and Dead Colocalize with Mitochondrial Outer Membrane Marker TOM20**
CHO cells transduced with MitoSTARD4 WT or MitoSTARD4 Dead**.** A) Immunoblot analysis of CHO cell lysates, probed with anti-V5 epitope tag. Actin was used as a loading control, 10 μg protein per lane. B) Immunofluorescence using antibodies against Tom20 and V5 epitope. C) Filipin staining and immunofluorescence using anti-Tom20 antibody. Scale bars 10 μm.

3.2.4 Mitochondrial Cholesterol and Cholesterol Import are Increased by MitoSTARD4 Expression

To investigate whether mitochondrial cholesterol content is altered by MitoSTARD4 expression, I performed subcellular fractionation by density gradient ultracentrifugation to isolate purified mitochondria (Charman et al, 2010). A density gradient of 10, 23 and 50 percent Percoll was used, endosomes were collected at the 0/10 and 10/23 interfaces and mitochondria collected at the 23/50% interface. Endosomes and lysosomes are similar in density to mitochondria and pose an issue of contamination. Mitochondria purity was determined via immunoblotting for NPC1, an endosomal protein and VDAC1, a mitochondrial protein on immunoblots of 5 μg protein from lysate and endosomal fraction and 15 μg protein from lysate of mitochondrial fractions (Figure 3.05 A). Some NPC1 was apparent in the mitochondrial fractions of both MitoSTARD4 WT and MitoSTARD4 dead samples, with three times more NPC1 immunoreactivity in the MitoSTARD4 dead (Figure 3.05 A). MitoSTARD4 dead also had a different distribution of NPC1 immunoreactivity in the endosomal fractions, with less in the upper endosomal fraction and more in the lower endosomal fraction, than MitoSTARD4 WT (Figure 3.05 A). VDAC was present in the mitochondrial fractions of both MitoSTARD4 WT and MitoSTARD4 Dead at a similar amount and was minimally present in the lysosomal fractions. Mitochondrial cholesterol was elevated in MitoSTARD4 WT over Dead (Figure 3.05 B), suggesting that STARD4 anchored to the cytosolic side of the mitochondrial outer membrane can transfer cholesterol into the membrane and increase total mitochondrial cholesterol content. NPC1 bands in the mitochondrial

fractions indicated lysosomal contamination of the mitochondria. MitoSTARD4 Dead appeared to have more NPC1 immunoreactivity than MitoSTARD4 WT (Figure 3.05 A). Given that lysosomal contamination would likely elevate cholesterol content, the cholesterol increase in MitoSTARD4-WT mitochondria may be even higher than measured in our fractions.

In NPC1-deficient CHO cells, only mitochondrial cholesterol content is increased, but not transport of cholesterol to the inner mitochondrial membrane, suggesting that the accumulation of mitochondrial cholesterol is in the mitochondrial outer membrane (Charman et al., 2010). To investigate whether cholesterol delivered to mitochondria by MitoSTARD4 reaches the inner mitochondrial membrane, we used CHO cells stably expressing a CYP11A1 fusion protein that catalyzes the conversion of cholesterol to pregnenolone at the inner mitochondrial membrane (Kennedy et al., 2017). Pregnenolone production was 1.7-fold higher in MitoSTARD4 WT, compared to MitoSTARD4 Dead (Figure 3.06 A), indicating increased import of cholesterol to the inner mitochondrial membrane. Maximal F2 activity was determined by treatment with 22-OH cholesterol, which freely crosses the mitochondrial membranes and is a substrate for the F2 fusion protein. Maximal activity of the F2 fusion protein was equal for both MitoSTARD4 and MitoSTARD4 Dead and was over 20-fold higher than pregnenolone from endogenous cholesterol (Figure 3.06 B). This indicates that the difference in pregnenolone production by the MitoSTARD4 system is not due to changes in F2 expression or activity, and that transport to the inner mitochondrial membrane is the limiting step under these conditions.

A

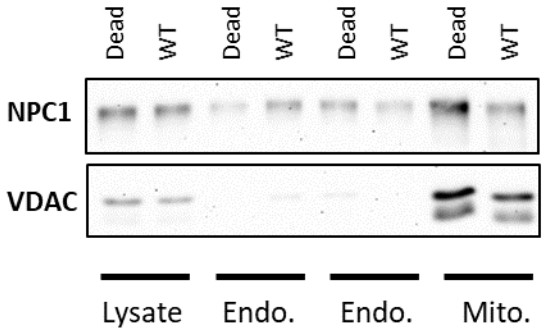
Dead
WT
Dead
WT
Dead
WT
Dead
WT
NPC1
VDAC
Lysate
Endo.
Endo.
Mito.

B

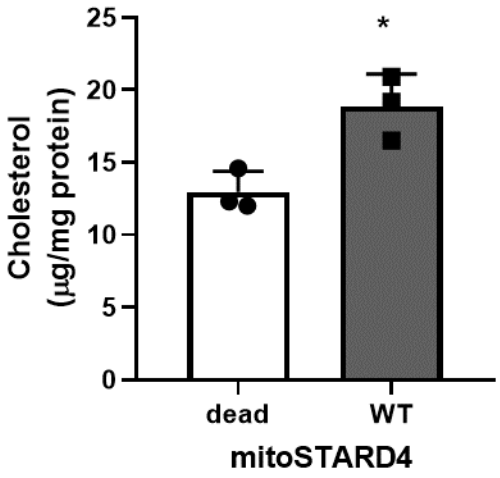
Cholesterol (µg/mg protein)
25
20
15
10
5
0
*
dead
WT
mitoSTARD4

Figure 3.05 **MitoSTARD4 Expression Increases Mitochondrial Cholesterol Content**

CHO cells were transduced with MitoSTARD4 WT or MitoSTARD4 Dead. A) Immunoblot analysis of lysates, endosomal fractions (Endo.) (top fraction left, lower fraction right) or mitochondrial fractions (Mito.) probed with anti-NPC1 and anti-VDAC1 antibodies on the same membrane. B) Cholesterol content of mitochondrial fractions. Mean of three independent experiments ± SEM. *$p < 0.05$.

A

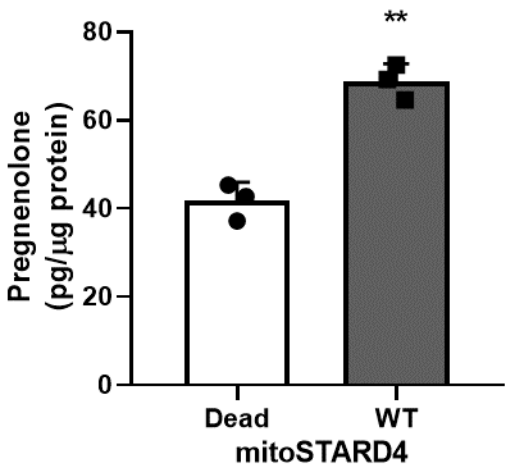
**
80
60
40
20
0
Pregnenolone
(pg/µg protein)
Dead
WT
mitoSTARD4

B

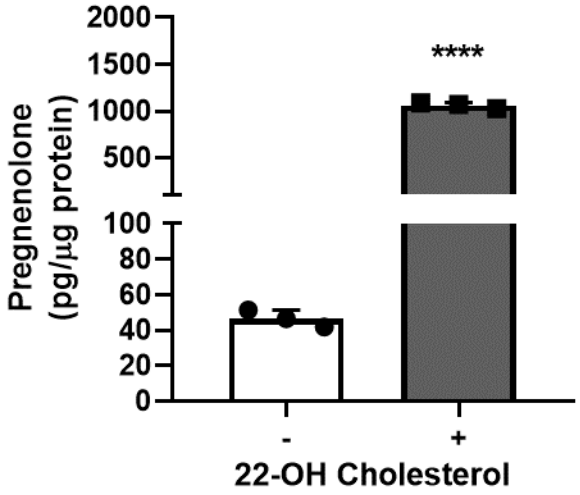
****
2000
1500
1000
500
100
80
60
40
20
0
Pregnenolone
(pg/µg protein)
-
+
22-OH Cholesterol

Figure 3.06 **MitoSTARD4 Expression Increases Import of Cholesterol to the Inner Mitochondrial Membrane**
CYP11A1 fusion protein expressing cells, medium was collected after a 24 h incubation and pregnenolone was measured. A) Cells transduced with MitoSTARD4 WT or MitoSTARD4 Dead. B) Non-transduced cells with or without 5 μM 22-OH cholesterol treatment in the efflux medium, as indicated. Results are mean ± SD of three independent experiments in triplicate. *$p < 0.05$, ****$p < 0.0001$ MitoSTARD4 WT vs MitoSTARD4 Dead.

3.3 Metabolic Consequences of Increased Mitochondrial Cholesterol

3.2.1 Lactate Production is Increased with Mitochondrial Cholesterol Elevation

Lactate production is increased in both the NPC1-deficient CHO cells, NPC1-deficient brain and in some cancers (Kennedy et al., 2014, Goodwin et al., 2015). To determine whether the increase in lactate is due to increased mitochondrial cholesterol, I measured lactate production in MitoSTARD4 WT and MitoSTARD4 Dead infected CHO cells. Lactate production was increased in MitoSTARD4 WT expressing cells over Dead (Figure 3.07 A). Addition of the pyruvate dehydrogenase kinase inhibitor, dichloroacetate (DCA), which relieves inhibition of pyruvate dehydrogenase, decreased lactate production in both MitoSTARD4 WT and Dead expressing cells. To investigate the role of oxidative stress in the increased lactate production, NAC, which acts as an antioxidant by providing cysteine for glutathione synthesis, was added 24h prior to applying efflux medium to the cells. NAC reduced lactate production in both MitoSTARD4 WT expressing cells and MitoSTARD4 Dead expressing cells and the difference between the two was not statistically significant. Since the difference in lactate production between MitoSTARD4 WT and MitoSTARD4 Dead expressing cells was removed by treatment with DCA, inhibition of pyruvate dehydrogenase in MitoSTARD4 WT may contribute to the increased lactate production.

3.3.2 Elevated Mitochondrial Cholesterol Elicits a Stress Response

Mitochondrial dysfunction is commonly associated with increased generation of reactive oxygen species and a resultant activation of antioxidant responses. Nuclear factor erythroid 2-related factor 2 (NRF2) upregulates the transcription of antioxidant proteins in response to increased oxidative stress, including upregulation of NRF2 itself (Tonelli et al., 2018). NRF2 mRNA levels were increased in MitoSTARD4 WT expressing cells over MitoSTARD4 Dead (Figure 3.07 B), similar to the increase in NRF2 mRNA in NPC1-deficient CHO cells (Kennedy et al., 2014). Increased NRF2 mRNA in the MitoSTARD4 WT expressing cells suggested that increased mitochondrial cholesterol induced an oxidative stress response.

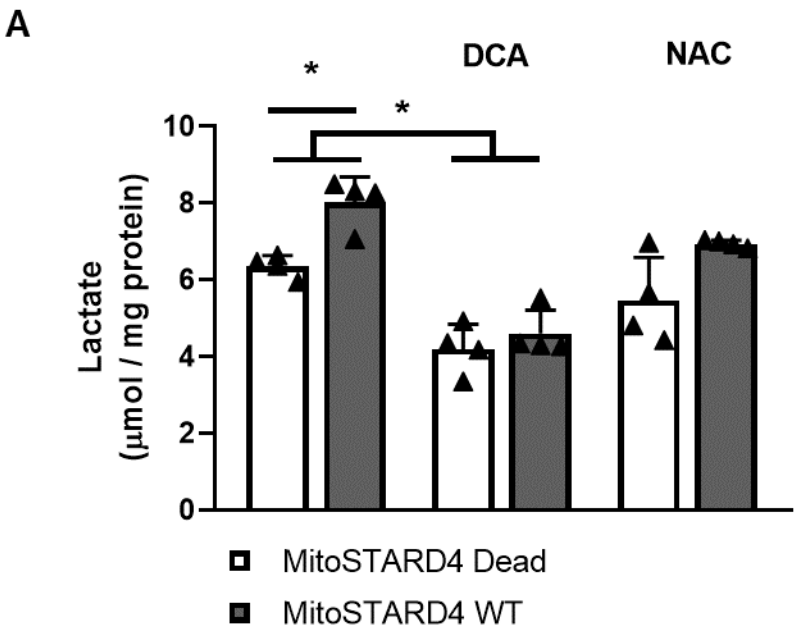
A
DCA
NAC
*
*
Lactate
(µmol / mg protein)
10
8
6
4
2
0
MitoSTARD4 Dead
MitoSTARD4 WT

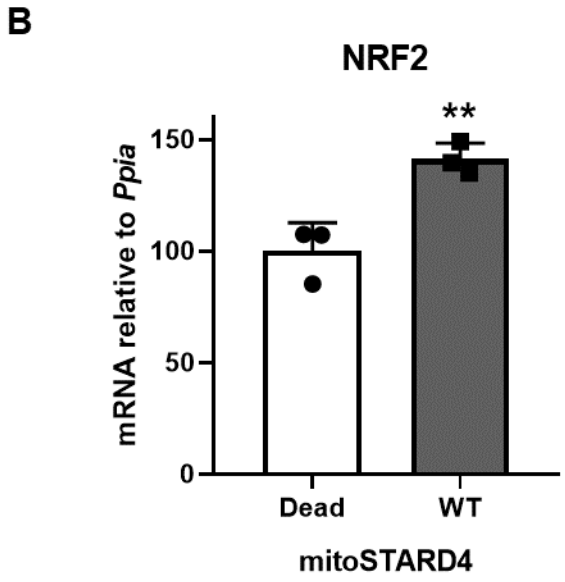
B
NRF2
**
mRNA relative to Ppia
150
100
50
0
Dead
WT
mitoSTARD4

Figure 3.07 **MitoSTARD4 Increases Lactate Production in CHO Cells and Induces a Stress Response**
CHO cells transduced with MitoSTARD4 WT or MitoSTARD4 Dead. A) Cells were incubated 4 h with or without 10 mM DCA or 24 h pre-treatment with 1 mM NAC, as indicated. Lactate was measured in the medium collected at the end of the 4 h incubation. Mean ± SD of three independent experiments in triplicate. B) NRF2 mRNA levels. *Ppia* was used as a reference gene. Mean ± SD of three independent experiments in duplicate. *$p < 0.05$, **$p < 0.01$ MitoSTARD4 WT vs MitoSTARD4 Dead.

3.4 Influence of Mitochondrial Cholesterol Content on the Associations of VDAC

3.4.1 Altered Protein Associations with Mitochondrial Fractions

Previous studies have explored the binding of cholesterol to VDAC (Weiser et al., 2014, Budelier et al., 2017). It has been suggested that cholesterol binding to VDAC may alter its interaction with other proteins (Pastorino and Hoek, 2008, Shoshan-Barmatz et al. 2017). To investigate this possibility, I assessed the differential mitochondrial association of known VDAC-interacting proteins in MitoSTARD4 WT and MitoSTARD4 Dead. CHO cells transduced with MitoSTARD4 WT or MitoSTARD4 Dead were lysed, and the lysates were separated by differential centrifugation into crude mitochondria and cytosol fractions of equivalent volume to lysate, cytosolic fractions containing ER and plasma membrane and cytosolic proteins. Immunoblotting was performed on lysates, crude mitochondria and cytosol for proteins known to interact with VDAC1, including BCL-XL, GRP75, PINK1 and PARKIN. Immunoblots were loaded with 20 μg lysate fraction, and equal volumes of cytosolic and mitochondrial fractions for equal protein loading between fractions. Protein staining was used to verify equivalent protein loading of fractions between MitoSTARD4 WT and MitoSTARD4 dead samples.

BCL-XL is an anti-apoptotic protein that binds to VDAC1 and prevents the binding of pro-apoptotic proteins and subsequent induction of apoptosis (Arbel, Ben-Hail and Shoshan-Barmatz, 2012). Glucose-regulated protein 75 (GRP75) is a tethering protein involved in the formation of mitochondria-ER contact sites,

binding VDAC1 on the mitochondria and inositol-1,4,5-trisphosphate-receptor 3 of the ER, playing a role in ER-mitochondria calcium transfer (Szabadkai et al., 2006). PINK1 is a mitophagy-regulating protein which is stably associated with VDAC1 on the outer mitochondrial membrane of depolarized mitochondria (Narendra and Youle, 2011). PINK1 recruits PARKIN, which binds to VDAC1 and ubiquitinates mitochondrial proteins (Narendra et al., 2008, Matsuda et al., 2010), which serves as the signal to begin mitophagy (Matsuda et al., 2010). All four of these proteins had increased presence in the mitochondrial fraction of MitoSTARD4 WT over MitoSTARD4 Dead expressing cells (Figure 3.08, Figure 3.09). This suggests that cholesterol positively influences their mitochondrial association.

Given the role of BCL-XL as an anti-apoptotic protein, I decided to explore the apoptosis susceptibility of MitoSTARD4 WT and MitoSTARD4 Dead expressing cells. Staurosporine was used to induce apoptosis and Caspase 3 cleavage was used as a marker of apoptosis. Caspase 3 is cleaved as part of the Caspase cascade leading to apoptosis, increased levels of cleaved Caspase 3 are indicative of apoptosis (Wolf et al., 1999). MitoSTARD4 Dead expressing cells had more cleaved Caspase 3 than MitoSTARD4 WT expressing cells (Figure 3.10), suggesting increased resistance of MitoSTARD4 WT to staurosporine-induced apoptosis, which agrees with the increased presence of BCL-XL on mitochondria in these cells.

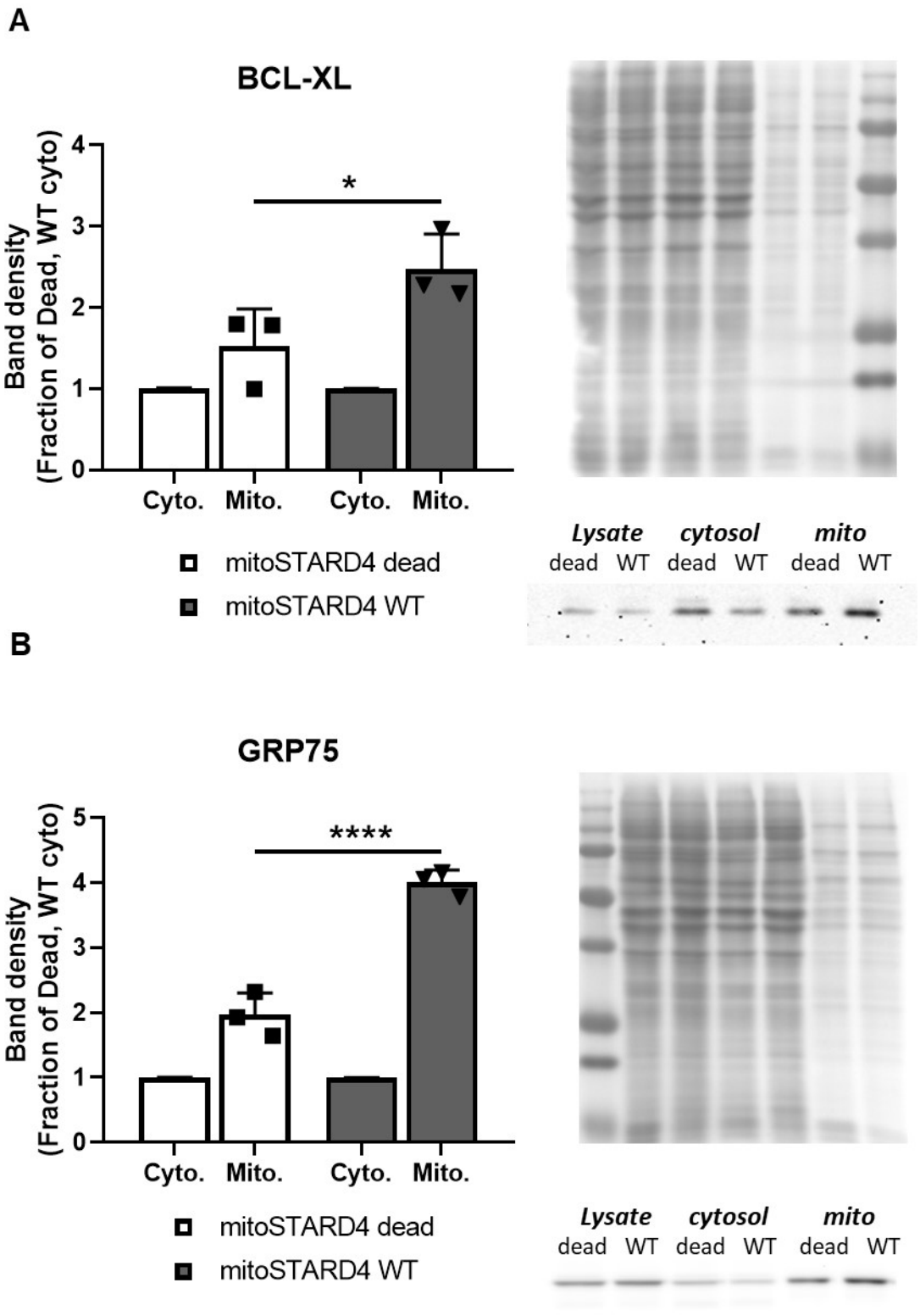
A
BCL-XL
Band density
(Fraction of Dead, WT cyto)
0
1
2
3
4
*
Cyto.
Mito.
Cyto.
Mito.
mitoSTARD4 dead
mitoSTARD4 WT
Lysate
cytosol
mito
dead
WT
dead
WT
dead
WT
B
GRP75
Band density
(Fraction of Dead, WT cyto)
0
1
2
3
4
5
****
Cyto.
Mito.
Cyto.
Mito.
mitoSTARD4 dead
mitoSTARD4 WT
Lysate
cytosol
mito
dead
WT
dead
WT
dead
WT

Figure 3.08 **Elevated Mitochondrial Cholesterol Influences Mitochondrial Association of BCL-XL, GRP75**
Representative immunoblots of lysates, crude mitochondrial fractions (mito.) or cytosolic fractions (cytosol) of CHO cells transduced with MitoSTARD4 Dead (dead) or MitoSTARD4 WT (WT), probed with anti-BCL-XL (A) or GRP75 (B) antibodies. Quantification of immunoblots, normalized to band density of the lysate. Reversible protein stain of immunoblots to show even protein loading. Mean of three independent experiments ± SD. *$p < 0.05$.

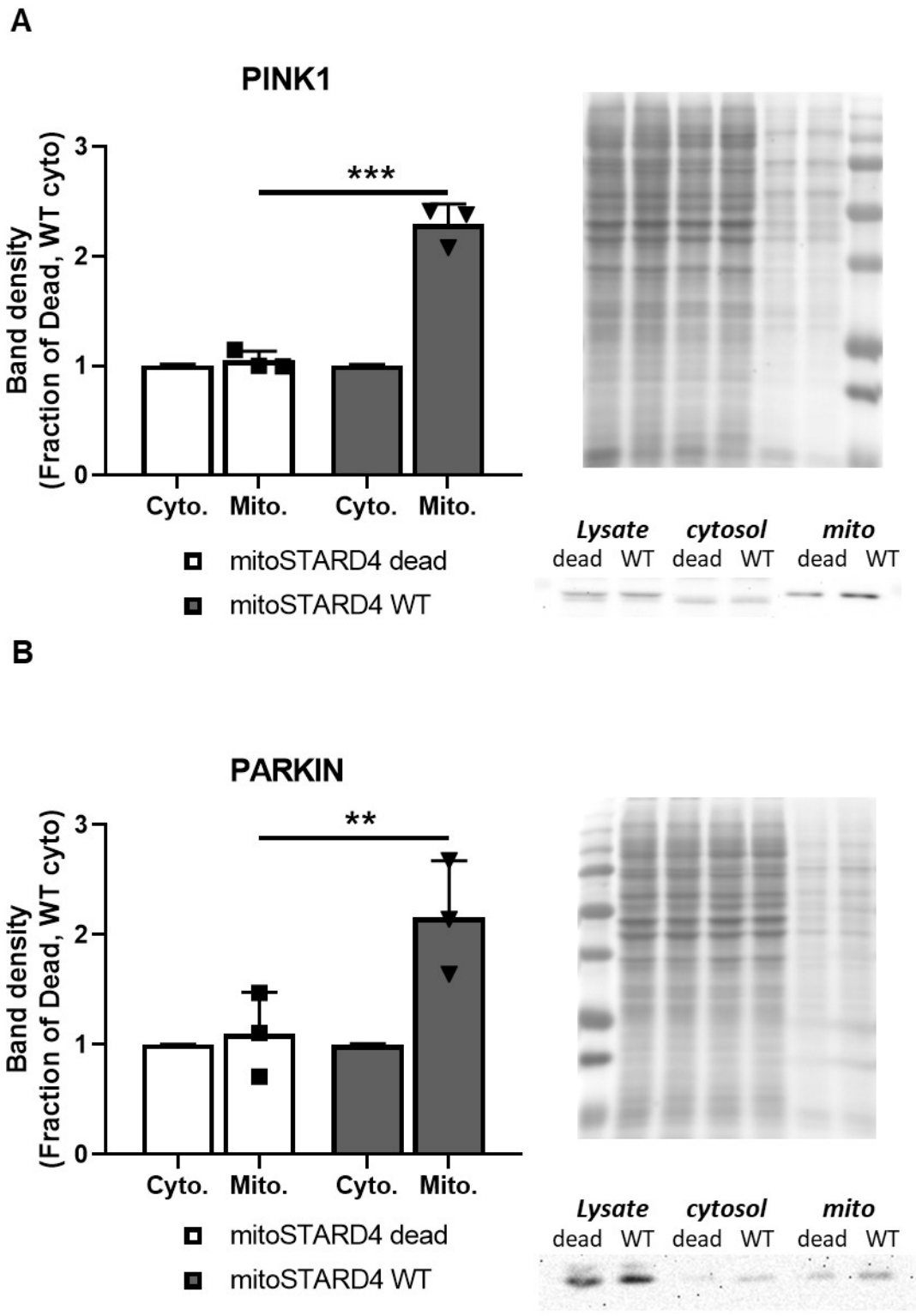
A
PINK1
Band density
(Fraction of Dead, WT cyto)
3
2
1
0
***
Cyto.
Mito.
Cyto.
Mito.
mitoSTARD4 dead
mitoSTARD4 WT
Lysate
cytosol
mito
dead
WT
dead
WT
dead
WT
B
PARKIN
Band density
(Fraction of Dead, WT cyto)
3
2
1
0
**
Cyto.
Mito.
Cyto.
Mito.
mitoSTARD4 dead
mitoSTARD4 WT
Lysate
cytosol
mito
dead
WT
dead
WT
dead
WT

Figure 3.09 **Elevated Mitochondrial Cholesterol Influences Mitochondrial Association of PINK1 and PARKIN**
Representative immunoblots of lysates, crude mitochondrial fractions (mito.) or cytosolic fractions (cytosol) of CHO cells transduced with MitoSTARD4 Dead (dead) or MitoSTARD4 WT (WT), probed with PINK1 (A) or PARKIN (B) antibodies. Quantification of immunoblots, normalized to band density of the lysate. Reversible protein stain of immunoblots to show even protein loading. Results are from three independent experiments.

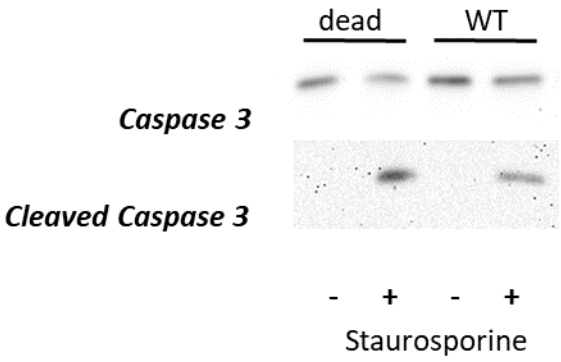
dead
WT
Caspase 3
Cleaved Caspase 3
- + - +
Staurosporine

Figure 3.10 **Elevated mitochondrial cholesterol increases resistance to staurosporine-induced apoptosis**
Immunoblot of CHO cell lysates transduced with MitoSTARD4 WT or MitoSTARD4 Dead, with or without 1 μM staurosporine for 18 h, probed with anti-Caspase 3 antibody.

3.4.2 VDAC1 FLAG Knock-in using CRISPR

Initially I wanted to perform co-immunoprecipitation of VDAC1 and its binding partners to determine if increased mitochondrial cholesterol could alter the protein associations of VDAC. Commercial antibodies do not recognize non-denatured VDAC and so immunoprecipitation was not an option. I decided to epitope-tag endogenous VDAC using CRISPR genome editing rather than plasmid-based ectopic expression, as overexpression of VDAC can result in mis-localization to the plasma membrane (Dubey, Godbole and Mathew, 2016). Overexpression of VDAC would also alter the ratio of VDAC to binding partners and potentially confound the results.

The pFETCh system described by Savic et al. (2015) was used for homology-directed repair knock-in of 3X FLAG epitope tag C-terminal to VDAC1 in CHO cells. This CRISPR system includes a P2A element and G418 resistance gene for selection of successful edits. The CRISPR tagged cell lines were screened for the insert by cDNA PCR of the edited region, and two were selected with monoallelic edits (Figure 3.11 A). The primers used for screening anneal outside of the homology arms, ensuring that integrated plasmid would not be amplified (Figure 3.11 B). The screening amplicons of the two monoallelic edits were sequenced and matched the *in silico* generated sequences (Appendix B). I performed immunoblotting on lysates from several potential CRISPR edited lines and unedited CHO cells to probe for the presence of VDAC and the FLAG epitope (Figure 3.11 C). The two edits 3-2-6 and 3-2-8 that were confirmed by sequencing both had distinct FLAG epitope bands at the

correct molecular weight but did not have a signal for VDAC at the wildtype or edited molecular weights (32 kDa and 38 kDa, respectively). Another potential clone, 3-2-3, had no signal for either VDAC or the FLAG epitope (Figure 3.11 C). A final clone tested, 3-3-2, had a sole band for VDAC, matching that of the unedited CHO cells (Figure 3.11 C). This suggests that the 3-2-6 and 3-2-8 lines were success not properly expressing edited VDAC or that edited VDAC was being degraded, while the 3-2-3 and 3-3-2 lines were unsuccessful edits. As the wildtype allele for VDAC1 did not produce a band on immunoblotting (Figure 3.11 C), this was potentially caused by a CAS9-induced frameshift mutation in that allele.

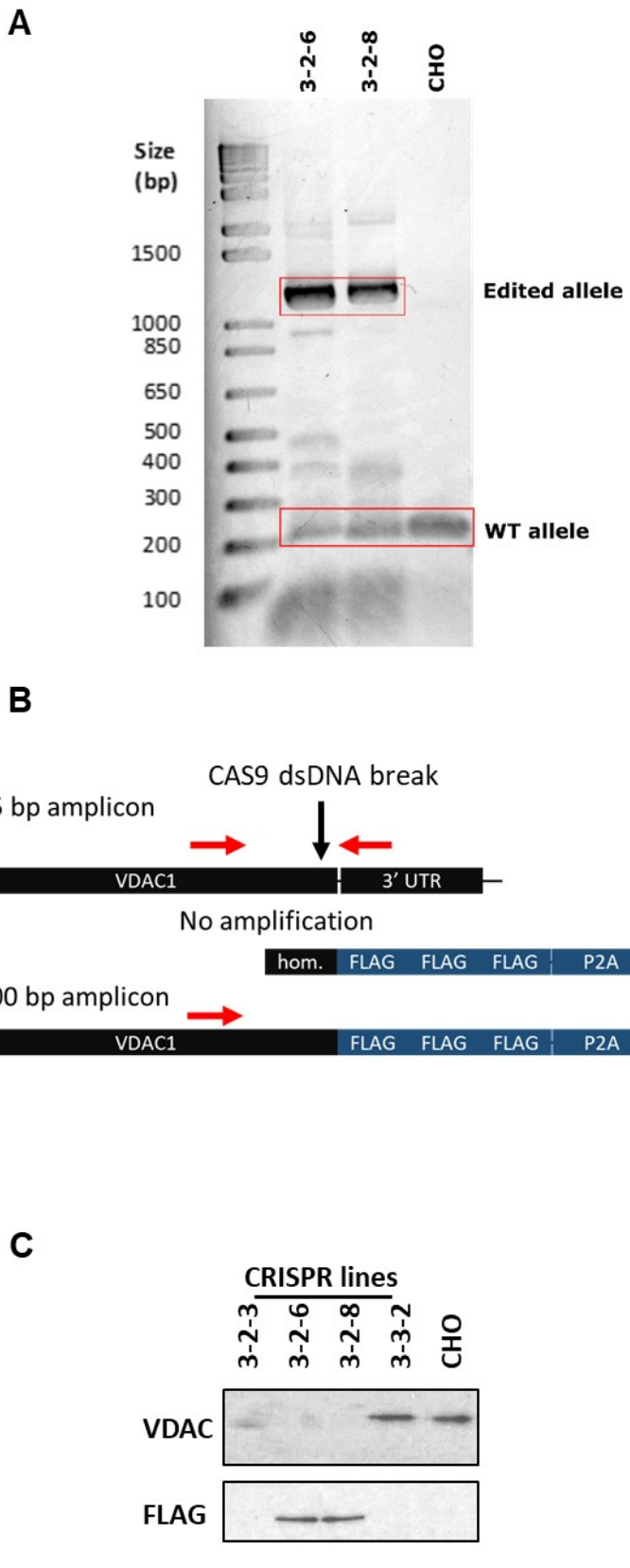
A
3-2-6
3-2-8
CHO
Size (bp)
1500
1000
850
650
500
400
300
200
100
Edited allele
WT allele
B
CAS9 dsDNA break
205 bp amplicon
VDAC1
3' UTR
No amplification
hom.
FLAG
FLAG
FLAG
P2A
NeoR
hom.
1200 bp amplicon
VDAC1
FLAG
FLAG
FLAG
P2A
NeoR
3' UTR
C
CRISPR lines
3-2-3
3-2-6
3-2-8
3-3-2
CHO
VDAC
FLAG

Figure 3.11 **CRISPR-Edited CHO Cells with Genomic VDAC1 Epitope Tag Insertion**
Monoclonal CHO cell lines CRISPR-edited with pFETCH plasmid system for VDAC1 carboxyl-terminal insert of 3x FLAG epitopes. A) Agarose gel electrophoresis of cDNA PCR products for screening of knock-in, depicting amplicons from edited and unedited alleles. B) Depiction wildtype CHO VDAC1 gene, homology-directed repair template and CRISPR-edited VDAC1, with annealing locations of screening primers (red arrows) and amplicon sizes. C) Immunoblot of potential CRISPR-edited monoclonal cell lines and unedited CHO cells, probed with anti-VDAC or anti-FLAG antibodies. 10 μg protein per lane.

CHAPTER 4: DISCUSSION

4.1 Acute Translocation of STARD4 to the Outer Mitochondrial Membrane

4.1.1 System for Acutely Increasing Mitochondrial Cholesterol

Initially this project aimed to produce an acute, inducible model of increased mitochondrial cholesterol. This model was based on the "knocksideways" system, whereby rapamycin binding domains, FRB and FKBP are fused to proteins of interest and rapamycin is used to induce colocalization of the two proteins (Robinson et al., 2010) (Figure 3.01). Using this system to sequester STARD4 to the mitochondrial outer membrane and explore the effect of STARD4 removal on cholesterol transport, Iaea *et al*. incidentally observed that mitochondria appeared to have increased cholesterol content as determined by filipin staining (Iaea et al., 2017). In the first part of my thesis I aimed to use this acute translocation model to determine whether it does increase mitochondrial cholesterol in SH-SY5Y neuroblastoma cells.

Acute translocation of STARD4 was presumed to work by directing cholesterol transport into the mitochondria by proximity of the cholesterol transport protein to the mitochondrial outer membrane. By inducing STARD4 localization to the mitochondria, cholesterol is acutely re-directed from a cellular source. As this system relies on rapamycin and two rapamycin binding domains to function, we made vectors missing one or the other to control for effects arising from their presence.

Initial validation experiments of this system showed that the translocation was functional with both binding domains present and rapamycin added, but translocation did not occur when missing either binding domain or in the absence of rapamycin (Figure 3.02 A), as expected. Filipin staining for unesterified cholesterol in STARD4-CIT transduced cells did not show the formation of peri-mitochondrial cholesterol-rich vesicles or other overt changes in cholesterol distribution, contrary to what was previously described (Iaea et al., 2017). Given that mitochondria have cholesterol 40-fold lower than other membranes, any visible changes would indicate a substantial increase in cholesterol. Iaea et al. used transient transfection with FuGENE 6 to express the STARD4-CIT system, while I used lentiviral transduction which commonly leads to lower levels of expression than transient transfection. This lower expression level my explain why we did not observe the aberrant localization of cholesterol in peri-mitochondrial vesicles as Iaea et al. did.

Lactate production was measured in cells expressing the STARD4-CIT system and was not changed by the translocation of STARD4 to mitochondria but was reduced in cells expressing STARD4+/-FKBP and OMM-FRB (Figure 3.03). From this, it appeared that the presence of the FRB domain was elevating lactate production. Alternatively, expression of FKBP without the FRB domain may be reducing lactate production. However, rapamycin treatment to induce STARD4 translocation did not change lactate production in STARD4+FKBP and OMM+FRB expressing cells. Previously, it was found that the oxidative stress response preceeds increased lactate production (Kennedy et al., 2014), so it is possible that in the four-hour acute time scale, there was not enough ROS production to increase

lactate production. The difference between this system may lie in the cell type used, human SH-SY5Y cancer cells versus hamster cells, or in the shorter timeframe.

Our experimentation with the acute system stopped at this point. With the possibility that rapamycin-binding domains would alter cellular metabolism on their own, it was considered too confounding to explore mitochondrial functionality and metabolism using this system.

The human neuroblastoma cell line, SH-SY5Y, was used with the acute translocation of STARD4 as our interest in mitochondrial cholesterol is based in neurodegenerative disease. SH-SY5Y cells can be differentiated into neuron-like cells, a useful model for studying a neuronal disease. However, the SH-SY5Y cell line proved to be a difficult cell model to use, as it is a heterogeneous cell population, and we were plagued with inconsistencies, slow growth and limited usable passages of the cells. When the decision was made to move to a medium-term model not dependent on FRB or FKBP domains, I used CHO cells for a more direct comparison to mitochondrial cholesterol increase induced by NPC1 deficiency.

4.2 Metabolic Consequences of Increased Mitochondrial Cholesterol

4.2.1 The MitoSTARD4 Model of Increased Mitochondrial Cholesterol

Moving on from the acute translocation of STARD4 to mitochondria, we generated vectors for constitutive expression of mitochondrial outer membrane targeted STARD4 (MitoSTARD4) as a chronic model of increased mitochondrial cholesterol (Figure 3.01). The MitoSTARD4 model is a fusion protein of STARD4

with an N-terminal mitochondrial targeting sequence that intercalates into the mitochondrial outer membrane, with STARD4 on the cytosolic side.

While this model does not reveal details of the acute impacts of mitochondrial cholesterol, it could still elucidate any effects that arise specifically from mitochondrial cholesterol. As a non-physiological system with overexpression of a protein intercalated into the mitochondrial outer membrane, a control was needed to account for any effects arising from the STARD4 fusion protein presence on the outer mitochondrial membrane and not from increased cholesterol. The W108D mutation of human STARD4 is unable to transfer cholesterol (Iaea et al., 2017) and therefore provided a good control for the MitoSTARD4 system, termed MitoSTARD4 Dead.

Elevation in mitochondrial cholesterol with the MitoSTARD4 system was comparable to that previously seen with NPC1-depleted CHO cells (Figure 3.05 B) (Kennedy et al., 2014). MitoSTARD4 WT also mediated the transfer of cholesterol to the inner mitochondrial membrane, as evidenced by the elevated pregnenolone production in MitoSTARD4 WT transduced cells also expressing the CYP11A1 fusion protein (Figure 3.06 A). The NPC1-deficient CHO cells had increased overall mitochondrial cholesterol, but not increased import (Charman et al., 2010). As CHO cells lack CYP11A1, in MitoSTARD4 WT-expressing cells it is expected that there will be accumulation in the outer mitochondrial membrane as the inner membrane becomes saturated.

4.2.1 Shift to Glycolysis in Cells with Elevated Mitochondrial Cholesterol

Increased lactate production is observed in several diseases with elevated mitochondrial cholesterol, including NPC disease and some cancers (Kennedy et al., 2014, Warburg, Wind and Negelein, 1927). Increased lactate production is due to increased glycolysis without a similar increase in oxidative phosphorylation or even a decrease in oxidative phosphorylation. Pyruvate from glycolysis can either be converted to acetyl-CoA for entry into the TCA cycle and feeding oxidative phosphorylation, or it can be converted to lactate to replenish NAD^+ and sustain glycolysis. Mitochondrial dysfunction has been noted in several neurodegenerative diseases (Bender et al., 2006, Bossy-Wetzel, Petrilli and Knott, 2008, Brown and Beal, 2004, Bubber et al., 2005), which results in increased glycolysis and lactate production to satisfy cellular energy requirements. Cancers also have increased lactate production even when oxygen supply is sufficient to continue supporting oxidative phosphorylation (Warburg, Wind and Negelein, 1927). Whether mitochondrial cholesterol influences glycolytic rates, either indirectly through effects on oxidative phosphorylation or through other mechanisms, is unknown. I used the MitoSTARD4 system to explore potential influences of mitochondrial cholesterol on lactate production and glycolytic rate. Lactate production was found to be increased with the MitoSTARD4 system (Figure 3.07 A), consistent with increased glycolysis with increased mitochondrial cholesterol. The increased lactate production was comparable to increased lactate seen in NPC1-deficient CHO cells. Co-depletion of STARD3 and NPC1 in CHO cells prevents mitochondrial cholesterol increase and also did not lead to increased lactate production (Kennedy et al., 2014,

Charman et al., 2010), suggesting that increased lactate production seen in NPC1-deficient CHO cells is due to the increase in mitochondrial cholesterol, rather than due to endosomal cholesterol accumulation. My observations in the MitoSTARD4 model further support this conclusion, because it does not have endosomal cholesterol accumulation detectable by filipin staining (Figure 3.04 C).

To further explore the cause for increased lactate production in the MitoSTARD4 expressing cells, I used the pyruvate dehydrogenase kinase inhibitor DCA (Stacpoole and Felts, 1970, Whitehouse, Cooper and Randle, 1974). Pyruvate dehydrogenase kinase phosphorylates and inhibits pyruvate dehydrogenase (Patel and Roche, 1990, Kolbova et al., 2001). Pyruvate dehydrogenase converts pyruvate into acetyl-CoA for the TCA cycle and subsequently mitochondrial oxidative phosphorylation. Addition of DCA reduced overall lactate production for both MitoSTARD4 WT and MitoSTARD4 Dead-expressing CHO cells and relieved the difference between them (Figure 3.07 A). The equal production of lactate when treated with DCA suggested that increased lactate production in untreated MitoSTARD4 WT expressing cells is due to inhibition of pyruvate dehydrogenase.

Previous studies in NPC1-deficient CHO cells showed that increased lactate production followed increased oxidative stress, and lactate production could be normalized following treatment with the NAC, which provides cysteine for glutathione synthesis (Kennedy et al., 2014). I measured lactate production in CHO cells expressing MitoSTARD4 WT or MitoSTARD4 Dead after treatment with NAC to determine whether lactate production is increased in part due to oxidative stress in

this system. Pre-treatment with NAC reduced lactate production for both MitoSTARD4 WT and MitoSTARD4 Dead cells, and they were not significantly different from each other (Figure 3.07 A), suggesting that oxidative stress plays a role in the increased glycolysis in this system. As DCA treatment also equalized lactate production for MitoSTARD4 WT and MitoSTARD4 dead, it is possible that oxidative stress and pyruvate dehydrogenase inhibition are connected. A possible mechanism for oxidative stress induced pyruvate dehydrogenase inhibition is through c-Jun N-terminal kinase (JNK), which is activated by ROS (Lo, Wong, Cruz, 1996). JNK activation and oxidative stress were shown to increase with aging in rat brain, with a concurrent increase in pyruvate dehydrogenase kinase, which phosphorylates and inactivates pyruvate dehydrogenase (Zhao et al., 2009) Pyruvate dehydrogenase activity also decreased with aging (Zhao et al., 2009). Further studies could address whether pyruvate dehydrogenase inhibition is involved by immunoblotting to determine the phosphorylation state of pyruvate dehydrogenase in MitoSTARD4 expressing cells, and whether this is altered by antioxidant treatment.

4.2.2 Oxidative Stress Response

Mitochondrial dysfunction can lead to increased reactive oxygen species production and increased oxidative stress, another process prominent in neurodegenerative disease (Bhat et al., 2015). The transcription factor NRF2 mediates expression of antioxidant response proteins, including HMOX1, NQO1, G6PDH, among others, and NRF2 itself. NRF2 is increased under conditions of mild

oxidative stress (Tonelli, Chio and Tuveson, 2018). Given the involvement of oxidative stress in neurodegenerative disease and the reduction in lactate production with antioxidant treatment, I wanted to explore oxidative stress in the MitoSTARD4 model, starting with NRF2 expression. NRF2 mRNA levels were increased in MitoSTARD4 WT expressing cells over MitoSTARD4 Dead (Figure 3.07 B). Increased NRF2 mRNA indicates increased oxidative stress in MitoSTARD4 WT expressing cells, suggesting mitochondrial dysfunction and reactive oxygen species production. To further strengthen the link between increased mitochondrial cholesterol and oxidative stress, reactive oxygen species production and the expression level of NRF2 target genes could be measured.

4.3 Comparison of MitoSTARD4 System to Disease Models

4.3.1 Similarities Among MitoSTARD4 Model, NPC1-Deficient CHO Cells and Cancers

The first aim of this thesis was to develop a model of increased mitochondrial cholesterol that does not have the drawbacks of disease-based models currently studied. NPC1-deficient CHO cells have increased mitochondrial cholesterol, as well as increased endosomal/lysosomal cholesterol (Charman et al., 2010). Cancers also have elevated mitochondrial cholesterol, but the reason for this is unknown (Grain, Clark and Harvey, 1983, Laurich et al., 2005, Houk et al., 2004, Baggetto, Glottes and Vial, 1992). MitoSTARD4 expression increased mitochondrial cholesterol without inducing accumulation in other cellular compartments that could be seen via filipin staining (Figure 3.04), and there are no other disease-induced changes, making it a

suitable model for the study of effects arising purely from increased mitochondrial cholesterol.

The MitoSTARD4 system successfully increased mitochondrial cholesterol levels and increased import of cholesterol to the inner mitochondrial membrane. The NPC1-deficient CHO cell model did not have increased mitochondrial cholesterol import to the inner mitochondrial membrane Charman et al., 2010). STARD1 mediates import of cholesterol from the outer mitochondrial membrane to the inner mitochondrial membrane (Clark et al., 1994). CHO cells lack STARD1, so it is possible that in NPC1-deficient CHO cells more cholesterol remains in the outer mitochondrial membrane, with insufficient capacity to import it to the inner mitochondrial membrane. Presumably, STARD4 on the mitochondrial outer membrane is able to act in the same manner as STARD1 and mediate the transfer of cholesterol from the outer membrane to the inner membrane. This hypothesis is supported by previous studies that ectopic expression of a STARD1 with an outer mitochondrial membrane targeting sequence increases mitochondrial cholesterol import (Bose et al., 2002). This fusion protein is similar to the MitoSTARD4 system, wherea START domain is anchored to the mitochondrial outer membrane on the cytosolic side via a leader sequence that intercalates into the outer mitochondrial membrane. Therefore, MitoSTARD4 may act in the same manner as STARD1. STARD3 mediates the transfer of endosomal cholesterol to mitochondria in the NPC1-deficient CHO cells, but does not increase import to the inner mitochondrial membrane. It is possible that the orientation of STARD3 in the endosomal membrane does not allow for the START domain to act in the same manner as

MitoSTARD4 or STARD1 and not allow for cholesterol import. In the placenta, which lacks STARD1, STARD3 seems to be responsible for mitochondrial cholesterol import (Esparza-Perusquía et al., 2015), and it was postulated that this process is mediated by cleavage of the START domain of STARD3, which allows for cholesterol import to occur (Esparza-Perusquía et al., 2015).

NPC1-deficient CHO cells and MitoSTARD4 WT expressing cells had similarly increased lactate production. In NPC1-deficient CHO cells, depletion of STARD3 reduces mitochondrial cholesterol elevation and normalized lactate production (Charman et al., 2010, Kennedy et al., 2014), suggesting that increased lactate production in NPC1-deficiency is due to elevated mitochondrial cholesterol, rather than due to other aspects of NPC disease. In both models, lactate production was normalized by treatment with DCA, suggesting that mitochondrial cholesterol increases inhibition of pyruvate dehydrogenase and induces increased glycolysis and lactate production. Antioxidant treatment also normalized lactate production in MitoSTARD4 WT expressing cells, and in NPC1-deficient CHO cells, suggesting a role of oxidative stress in the elevation of lactate production. Previously, it has been described that increased ROS leads to inhibition of pyruvate dehydrogenase and that ectopic expression of catalase or superoxide dismutase relieve pyruvate dehydrogenase inhibition, by clearance of ROS (Tabatabaie, Potts and Floyd, 1996). The elevated NRF2 levels in MitoSTARD4 WT expressing CHO cells with elevated mitochondrial cholesterol suggests increased ROS production, which may contribute to pyruvate dehydrogenase inhibition and increase in lactate production. Such a mechanism may also explain the lack of an increase in lactate production in

the acute STARD4-CIT model, as the short timeframe may not be long enough for a buildup of ROS to overwhelm normal oxidative stress response and inhibit pyruvate dehydrogenase.

4.4 Influence of Cholesterol on VDAC

4.4.1 VDAC1 CRISPR Knock-in

I used CRISPR/CAS9 gene editing to create CHO cells expressing endogenously FLAG tagged VDAC1 for the purpose of immunoprecipitation to explore the associations of VDAC1 under conditions of increased mitochondrial cholesterol (Figure 2.01). Two lines were monoallelic edits; however, VDAC protein levels were low in both lines (Figure 3.11 A, 3.11 C). Immunoblotting showed only faint FLAG bands and no VDAC band, corresponding to either the edited or unedited VDAC (Figure 3.11 C). Lack of a VDAC band suggests that the edit may be interfering with expression of the protein or inducing its degradation. To investigate the FLAG tagged VDAC, further experiments using proteasome inhibitors can be done to determine whether the protein is abnormally degraded.

4.4.2 Mitochondrial Associations of some VDAC-Interacting Proteins are Altered with Increased Mitochondrial Cholesterol

In lieu of immunoprecipitation of VDAC, I used crude mitochondria isolation to separate mitochondrial and cytosolic fractions. Immunoblotting was then used to determine relative amounts of specific proteins in the mitochondrial fraction. This method would not indicate whether a protein is more or less associated with VDAC

itself, but it would show if a known VDAC interacting protein is more or less mitochondrial.

PINK1 is imported and rapidly processed in polarized mitochondria. (Green et al., 2012). The final mature form of PINK1 is ubiquitinated and degraded (Deas et al., 2011, Liu et al., 2017). Proteolytic processing of PINK1 is inhibited in depolarized mitochondria, PINK1 is not degraded and remains bound VDAC1 on the outer mitochondrial membrane (Springer and Kahle, 2011, Lin et al., 2017, Lin and Beal, 2006). VDAC1-bound PINK1 recruits PARKIN, initiating ubiquitination of mitochondrial proteins, including VDAC1 itself. (Narendra et al., 2008, Matsuda et al., 2010), and signaling the induction of mitophagy (Matsuda et al., 2010). The PINK1/PARKIN process of mitophagy can be initiated by elevated ROS production, which serves to select for the degradation of dysfunctional mitochondria (Xiao et al., 2010). PINK1 and PARKIN were both increased in the mitochondrial fraction of cells with increased mitochondrial cholesterol, suggesting increased mitophagy and mitochondrial dysfunction (Figure 3.09 A, 3.09 B). The reactive oxygen species pathway for PINK1/PARKIN-induced mitophagy fits our findings of oxidative stress in cells with increased mitochondrial cholesterol. VDACs are essential for the recruitment of PARKIN to dysfunctional mitochondria (Sun et al., 2012), so it is possible that increased association with PINK1 and PARKIN in cells with elevated mitochondrial cholesterol is increasing induction of mitophagy. Enhanced mitophagy may increase the degradation of dysfunctional mitochondria and increase mitochondrial quality control.

GRP75 is a tethering protein that connects VDAC1 to inositol-1,4,5-trisphosphate-receptor 3 in the formation of ER-mitochondria contact sites (Szabadkai et al., 2006). ER-mitochondria contact sites are sites of transfer of calcium and lipids and have been proposed to have a role in cellular glucose homeostasis (Rieusset, 2018). GRP75 was increased in the mitochondrial fraction of MitoSTARD4 WT over MitoSTARD4 dead expressing cells, suggesting an increase in ER-mitochondria contact with increased mitochondrial cholesterol (Figure 3.08 B). Altered ER-mitochondria contact may alter calcium transfer to mitochondria, modulating the activity of metabolic enzymes.

BCL-XL was increased in mitochondrial fractions of MitoSTARD4 WT over MitoSTARD4 Dead-expressing cells (Figure 3.08 B). BCL-XL is anti-apoptotic when bound to VDAC, which would suggest that mitochondrial cholesterol may increase apoptosis resistance (Bertini et al., 2011). I then explored whether MitoSTARD4 WT expressing cells were resistant to staurosporine-induced apoptosis. MitoSTARD4 WT-expressing cells had reduced Caspase 3 cleavage when treated with staurosporine, indicating that the cells were less apoptotic than MitoSTARD4 Dead expressing cells. A previous study exploring the role of mitochondrial cholesterol in chemotherapy resistance found that by specifically reducing mitochondrial cholesterol by depletion of STARD1, cancer cells became more susceptible to chemotherapeutics (Montero et al., 2008). Our results that mitochondrial cholesterol increased apoptosis resistance support the hypothesis that increased mitochondrial cholesterol increases the resistance of cancer cells to apoptosis. This

result is also consistent with the increased association of anti-apoptotic BCL-XL in mitochondrial fractions.

CHAPTER 5: CONCLUSION

5.1 Conclusions

In this study, I propose that MitoSTARD4 is a novel model of elevated mitochondrial cholesterol that is appropriate for elucidating the effects of increased mitochondrial cholesterol in neurodegenerative diseases and cancers. I have also shown that mitochondrial cholesterol increases lactate production in a pyruvate dehydrogenase inhibition and oxidative stress dependent manner. This study has also shown that mitochondrial localization of some VDAC interacting proteins are modulated by mitochondrial cholesterol. It is my hope that these findings contribute to the understanding of neurodegenerative diseases.

BIBLIOGRAPHY

Abd-Elaziz, M., Moriya, T., Akahira, J., Suzuki, T., Sasano, H. (2005) StAR and progesterone producing enzymes (3β-hydroxysteroid dehydrogenase and cholesterol side-chain cleavage cytochromes P450) in human epithelial ovarian carcinoma: Immunohistochemical and real-time PCR studies. *Cancer Sci.* doi.org/10.1111/j.1349-7006.2005.00040.x

Almahbobi, G., Williams, L., Han, X., Hall, P. (1993) Binding of lipid droplets and mitochondria to intermediate filaments in rat Leydig cells. *J Reprod Fertil.* 98, 209-217.

Alpy, F., Latchumanan, V., Kedinger, V., Janoshazi, A., Thiele, C., Wendling, C., Rio, M-C., Tomasetto, C. (2005) Functional characterization of the MENTAL domain. *J Biol Chem.* 280, 17945–17952.

Alpy, F., Rousseau, A., Schwab, Y., Legueux, F., Stoll, I., Wendling, C., Spiegelhalter, C., Kessler, P., Mathelin, C., Rio, M-C., Levine, T., Tomasetto, C. (2013) STARD3 or STARD3NL and VAP form a novel molecular tether between late endosomes and the ER. *J Cell Sci.* 126, 5500–5512.

Alpy, F., Stoeckel, M., Dierich, A., Escola, J., Wendling, C., Chenard, M., Vanier, M., Gruenberg, J., Tomasetto, C., Rio, M-C. (2001) The steroidogenic acute regulatory protein homolog MLN64, a late endosomal cholesterol-binding protein. *J Biol Chem.* 276, 4261–4269.

Andersson, S., Davis, D., Dahlback, H., Jornvall, H., Russell, D. (1989) Cloning, structure, and expression of the mitochondrial cytochrome P-450 sterol 26-hydroxylase, a bile acid biosynthetic enzyme. *J Biol Chem.* 264(14), 8222-8229.

Arenas, F., Garcia-Ruiz, C., Fernandez-Checa, J. (2017) Intracellular cholesterol trafficking and impact in neurodegeneration. Front Mol Neurosci. 10(382), doi: 10.3389/fnmol.2017.00382.

Arakane, F., Kallen, C., Watari, H., Foster, J., Sepuri, N., Pain, D., Stayrook, S., Lewis, M., Gerton, G., Strauss, J. (1998) The mechanism of action of steroidogenic acute regulatory protein (StAR). StAR acts on the outside of mitochondria to stimulate steroidogenesis. *J Biol Chem*. 273, 16339–16345.

Arkane, F., Sugawara, T., Nishino, H., Liu, Z., Holt, J., Pain, D., Stocco, D., Miller, W., Strauss, J. (1996) Steroidogenic acute regulatory protein (StAR) retains activity in the absence of its mitochondrial import sequence: implications for the mechanism of StAR action. *PNAS*. 93, 13731-13736.

Artemenko, I., Zhao, D., Hales, D., Hales, K., Jefcoate, C.(2001) Mitochondrial Processing of Newly Synthesized Steroidogenic Acute Regulatory Protein (StAR), but Not Total StAR, Mediates Cholesterol Transfer to Cytochrome P450 Side Chain Cleavage Enzyme in Adrenal Cells. *J Biol Chem*. 276(49), 46583-46596.

Baggetto, L., Glottes, E., Vial, E. (1992) Low Mitochondrial Proton Leak Due to High Membrane Cholesterol Content and Cytosolic Creatine Kinase as Two Features of the Deviant Bioenergetics of Ehrlich and AS30-D Tumor Cells. *Cancer Res*. 52, 4935, 4941.

Bayrhuber, M., Meins, T., Habeck, M., Becker, S., Giller, K., Villinger, S., Vonrhein, C., Griesinger, C., Zweckstetter, M., Zeth, K. (2008) Structure of the human voltage-dependent anion channel. *PNAS.* 105(40), 15370-15375.

Bender, A., Krishnan, K., Morris C., Taylor G., Reeve A., Perry R., Jaros E., Hersheson J., Betts J., Klopstock T., et al. (2006) High levels of mitochondrial DNA deletions in substantia nigra neurons in aging and Parkinson disease. *Nat Genet.* 38, 515–517.

Bender, A., Schwarzkopf, R., McMillan, A., Krishnan K., Rieder, G., Neumann, M., Elstner, M., Turnbull, D., and Klopstock, T. (2008) Dopaminergic midbrain neurons are the prime target for mitochondrial DNA deletions. *J Neurol.* 255, 1231–1235.

Bertini, I., Chevance, S., Del Conte, R., Lalli, D., Turano, P. (2011) The Anti-Apoptotic Bcl-xL Protein, a New Piece in the Puzzle of Cytochrome C Interactome. *PLoS ONE* 6(4): e18329. https://doi.org/10.1371/journal.pone.0018329

Betaneli, V., Petrov, E., Schwille, P. (2012) The Role of Lipids in VDAC oligomerization. *Biophys J.* 102(3), 523-531.

Bloom, M., Evans, E., Mouritsen, O. (1991) Physical properties of the fluid-bilayer component of cell membranes: a perspective. *Q Rev Biophys.* 24, 293-297.

Bose, H., Lingappa, V., Miller, W. (2002) Rapid regulation of steroidogenesis by mitochondrial protein import. *Nature*. 417(6884), 87-91.

Bose, H., Lingappa, V., Miller, W. (2002) The steroidogenic acute regulatory protein, StAR, works only at the outer mitochondrial membrane. *Endocr Res.* 28, 295-308.

Bose, M., Whittal, R., Miller, W., Bose, H. (2008) Steroidogenic activity of StAR requires contact with mitochondrial VDAC1 and phosphate carrier protein. *J Biol Chem.* 283, 8837-8845.

Bossy-Wetzel, E., Petrilli, A., and Knott, A. (2008) Mutant huntingtin and mitochondrial dysfunction. *Trends Neurosci.* 31, 609 – 616.

Briggs, M., Yokoyama, C., Wang, X., Brown, M., Goldstein, J. (1993) Nuclear protein that binds sterol regulatory element of low density lipoprotein receptor promoter I. Identification of the protein and delineation of its target nucleotide sequence. *J Biol Chem*. 268, 14490-14496.

Brown, E., Albers, M., Shin, T., Ichikawa, K., Keith, C., Lane, W., Schreiber, S. (1994) A mammalian protein targeted by G1-arresting rapamycin-receptor complex. *Nature.* 369(6483), 756-758.

Brown, M., Goldstein, J. (1986) A Receptor-Mediated Pathway for Cholesterol Homeostasis. *Science.* 232(4746), 34-47.

Brown, M., Goldstein, J. (1999) A proteolytic pathway that controls the cholesterol content of membranes, cells and blood. *PNAS*. 96, 11041-11048.

Brown, M., Kovanen, P., Goldstein, J. (1979) Receptor-mediated uptake of lipoprotein-cholesterol and its utilization for steroid synthesis in the adrenal cortex. *Recent Prog Horm Res.* 35, 215-275.

Browne, S., and Beal, M. (2004) The energetics of Huntington's disease. *Neurochem Res.* 29, 531–546.

Bubber, P., Haroutunian, V., Fisch, G., Blass, J., Gibson, G. (2005) Mitochondrial abnormalities in Alzheimer brain: mechanistic implications. *Ann Neurol.* 57, 695– 703.

Budelier, M., Cheng, W., Bergdoll, L., Chen, Z., Janetka, J., Abramson, J., Krishnan, K., Mydock-McGrane, L., Covey, D., Whitelegge, J., Evers, A. (2017) Photoaffinity labeling with cholesterol analogues precisely maps a cholesterol-binding site in voltage-dependent anion channel-1. *J Biol Chem*. 292, 9294-9304.

Cafforio, P., Dammacco, F., Gernone, A., Silvestris, F. (2005) Statins activate the mitochondrial pathway of apoptosis in human lymphoblasts and myeloma cells. *Carcinogenesis*. 26(5), 883-891.

Camargo, F., Erickson, R., Garver, W., Hossain, G., Carbone, P., Heidenreich, R., Blanchard, J. (2001) Cyclodextrins in the treatment of a mouse model of Niemann-Pick C disease. *Life Sci.* 70(2), 131-142.

Campbell, A., Chan, S. (2008) Mitochondrial membrane cholesterol, the voltage dependent anion channel (VDAC), and the Warburg effect. *J Bioen Biomemb.* 40(3), 193-197.

Cardwell, C., Hicks, B., Hughes, C., Murray, L. (2014) Statin use after colorectal cancer diagnosis and survival: a population-based cohort study. *J Clin Oncol.* 32, 3177–3183.

Carstea, E., Morris, J., Coleman, K., Loftus, S., Zhang, D., Cummings, C., … , Tagle, D. (1997) Niemann-Pick C1 disease gene: homology to mediators of cholesterol homeostasis. *Science*. 277(5323), 228-231.

Carstea, E., Polymeropoulos, M., Parker, C., Detera-Wadleigh, S., O'Neill, R., Patterson, M., …, Vanier, M. (1993) Linkage of Niemann-Pick disease type C to human chromosome 18. *PNAS* 90(5) 2002–2004.

Chang, C., Lee, C., Chang, E., Cruz, J., Levesque, M., Chang, T. (1998) Recombinant acyl-CoA:cholesterol acyltransferase-1 (ACAT-1) purified to essential homogeneity utilizes cholesterol in mixed micelles or in vesicles in a highly cooperative manner. *J Biol Chem*. 273, 35132–35141.

Chang, T., Chang, C., Lin, S., Yu, C., Li, B., Miyazaki, A. (2001) Roles of acyl-coenzyme A:cholesterol acyltransferase-1 and -2. *Curr Opin Lipidol.* 12, 289-296.

Charman, M., Kennedy, B., Osborne, N., Karten, B. (2010) MLN64 mediates egress of cholesterol from endosomes to mitochodnria in the absence of functional Niemann-Pick Type C1 protein. J Lipid Res. 51, 1023-1034.

Charman, M., Kennedy, B., Osborne, N., Karten, B. (2010) MLN64 mediates egress of cholesterol from endosomes to mitochondria in the absence of functional Niemann-Pick Type C1 protein. *J Lipid Res*. 51(5), 1023-1034.

Colombini, M. (1979) Candidate for the permeability pathway of the outer mitochondrial membrane. *Nature*. 279, 643-645.

Colombini, M. (1989) Voltage gating in the mitochondrial channel, VDAC. *J Membr Biol*. 111, 103-111.

Colombini, M.(1980) Pore-size and properties of channels from mitochondria isolated from Neurospora-crassa. *J Membr Biol*. 53, 79-84.

Corvera, E., Mouritsen, O., Singer, M., Zuckerman, M. (1992) The permeability and the effect of acyl chain length for phospholipid bilayers containing cholesterol: theory and experiment. *Biochim Biophys Acta*. 1107, 261-270.

Deas, E., Plun-Favreau, H., Gandhi, S., Desmond, H., Kjaer, S., Loh, S., Renton, A., Harvey, R., Whitworth, A., Martins, M., Andrey, A., Wood, W. (2011) PINK1 cleavage at position A103 by the mitochondrial protease PARL. *Hum Mol Genet*. 20(5), 867-879.

Deffieu, M., Pfeffer, S. (2011) Niemann-Pick type C 1 function requires lumenal domain residues that mediate cholesterol-dependent NPC2 binding. *PNAS*. 108(47), 18932–18936.

Dolder, M., Wendt, S., Wallimann, T. (2001) Mitochondrial creatine kinase in contact sites: interaction with porin and adenine nucleotide translocase, role in permeability transition and sensitivity to oxidative damage. *Biol Signals Recept.* 10, 93–111.

Düvel, K., Yecies, J., Menon, S., Raman, P., Lipovsky, A., Souza, A., Triantafellow, E., Ma, Q., Gorski, R., Cleaver, S., Vander Heiden, M., MacKeigan, J., Finan, P., Clish, C., Murphy, L., Manning, B. (2010) Activation of a Metabolic Gene Regulatory Network Downstream of mTOR Complex 1. *Mol Cell.* 39(2), 171-183.

Dyson, M., Jones, M., Kowalewski, P., Manna, M., Alonso, M., Gottesman, M., Stocco, D. (2008) Mitochondrial A-kinase anchoring protein 121 binds type II protein kinase A and enhances steroidogenic acute regulatory protein-mediated steroidogenesis in MA-10 mouse leydig tumor cells. *Biol Reprod*. 78, 267–277.

Espenshade, P., Li, W., Yabe, D. (2002) Sterols block binding of COPII proteins to SCAP, thereby controlling SCAP sorting to ER. *PNAS*. 99(18) 11694-11699.

Evans, M., Finean, J. (1965) The lipid composition of myelin from brain and peripheral nerve. *J Neurochem*. 12, 729-734.

Fernandez, A., Llacuna, L., Fernandez-Checa, J,. Colell, A. (2009) Mitochondrial cholesterol loading excerabates amyloid beta peptide-induced inflammation and neurotoxicity. *J Neurosci.* 29, 6394-6405.

Geisler, S., Holmström, K., Skujat, D., Fiesel, F., Rothfuss, O., Kahle, P., Springer, W. (2010) PINK1/Parkin-mediated mitophagy is dependent on VDAC1 and p62/SQSTM1. *Nat Cell Biol*. 12, 119–131.

Goritz, C., Mauch, D., Pfrieger, F. (2005) Multiple mechanisms mediate cholesterol-induced synaptogenesis in a CNS neuron. *Mol Cell Neuro.* 29(2), 190-201.

Grain, R., Clark, R., Harvey, B. (1983) Role of Lipid Transfer Proteins in the Abnormal Lipid content of Morris Hepatoma Mitochondria and Microsomes. *Cancer Res.* 43, 3197-3202.

Greene, A., Grenier, K., Aguileta, M., Muise, S., Farazifard, R., Haque, M., McBride, H., Park, D., Fon, E. (2012) Mitochondrial processing peptidase regulates PINK1 processing, import and Parkin recruitment. *EMBO Rep.* 13(4), 378-385.

Gurnev, P., Rostovtseva, T., Bezrukov, S. (2011) Tubulin-blocked state of VDAC studied by polymer and ATP partitioning. *FEBS Lett.* 585, 2363–2366.

Haines, T. (2001) Do sterols reduce proton and sodium leaks through lipid bilayers? *Prog Lipid Res*. 40, 299-324.

Hall P., Young D. (1968) site of action of trophic hormones upon the biosynthetic pathways to steroid hormones. *Endocrinology.* 82, 559–565.

Hanada, K., Kumagai, K., Yasuda, S., Miura, Y., Kawano, M., Fukasawa, M., Nishijima, M. (2003) Molecular machinery for non-vesicular trafficking of ceramide. *Nature.* 426, 803-809.

Hao, M., Lin, S., Karylowski, O., Wüstner, D., McGraw, T., Maxfield, F. (2002) Vesicular and non-vesicular sterol transport in living cells. *J Biol Chem*. 277(1), 609-617.

Hayashi, T., Rizzuto, R., Hajnoczky, G., Su, T. (2009) MAM: more than just a housekeeper. *Trends Cell Biol*. 19, 81–88.

Horton, J., Goldstein, J., Brown, M. (2002) SREBPs: activators of the complete program of cholesterol and fatty acid synthesis in the liver. *J Clin Invest*. 109, 1125-1131.

Horton, J., Shah, N., Warrington, J., Anderson, N., Park, S., Brown, M., Goldstein, J. (2003) Combined analysis of oligonucleotide microarray data from transgenic and knockout mice identifies direct SREBP target genes. *PNAS*. 100, 12027– 12032.

Houk, C., Pearson, E., Martinelle, N., Donahoe, P., Teixeira, J. (2004) Feedback Inhibition of Steroidogenic Acute Regulatory Protein Expression in Vitro and in Vivo by Androgens. *Endocrinology*. 145(3), 1269–1275.

Hua, X., Sakai, J., Brown, M., Goldstein, J. (1996) Regulated cleavage of sterol regulatory element binding proteins (SREBPs) requires sequences on both sides of the endoplasmic reticulum membrane. *J Biol Chem*. 271, 10379-10384.

Hua, X., Sakai, J., Ho, Y., Goldstein, J., Brown, M. (1995) Hairpin orientation of sterol regulatory element binding protein-2 in cell membranes as determined by protease protection. *J Biol Chem*. 270, 29422-29427.

Hua, X., Sakai, J., Ho, Y., Goldstein, J., Brown, M. (1995-2) Hairpin orientation of sterol regulatory element-binding protein-2 in cell membranes as determined by protease protection, J. Biol. Chem. 270 (1995) 29422–29427.

Hua, X., Wu, J., Goldstein, J., Brown, M., Hobbs, H. (1995-1) Structure of the human gene encoding sterol regulatory element binding protein-1 (SREBF1) and

localization of SREBF1 and SREBF2 to chromosomes 17p11.2 and 22q13. *Genomics.* 25, 667–673.

Hua, X., Yokoyama, C., Wu, J., Briggs, M., Brown, M., Goldstein, J., Wang, X. (1993) SREBP-2, a second basic-helix-loop-helix-leucine zipper protein that stimulates transcription by binding to a sterol regulatory element. *PNAS*. 90(24), 11603-11607.

Iaea, D., Mao, S., Lund, F., Maxfield, F. (2017) Role of STARD4 in sterol transport between the endocytic recycling compartment and the plasma membrane. *Mol Biol Cell*. 28, 1111-1122.

Infante R., Wang, M., Radhakrishnan, A., Kwon, H., Brown, M., Goldstein, J. (2008) NPC2 facilitates bidirectional transfer of cholesterol between NPC1 and lipid bilayers, a step in cholesterol egress from lysosomes. *PNAS*. 105(40), 15287–15292.

Issop, L., Rone, M., Papadopoulos, V. (2012) Organelle plasticity and interactions in cholesterol transport and steroid biosynthesis. *Mol Cell Endocrinol*.

Jacobs, E., Newton, C., Thun. M., Gapstur, S. (2011) Long-term use of cholesterol-lowering drugs and cancer incidence in a large United States cohort. *Cancer Res.* 71, 1763–1771.

Karten, B., Peake, K., Vance, J. (2009) Mechanisms and consequences of impaired lipid trafficking in Niemann-Pick type C1-deficient mammalian cells. *Biochim Biophys Acta.* 1791, 659-670.

Kayser, H., Kratzin, H., Thinnes, F., Gotz, H., Schmidt, W., Eckart, K., Hilschmann, N. (1989) To the knowledge of human porins. 2. Characterization and primary structure of a 31-kDa porin from human b-lymphocytes (porin 31 HL). *Biol Chem*. 370, 1265-1278.

Keinan, N., Tyomkin, D., Shoshan-Barmatz, V. (2010) Oligomerization of the Mitochondrial Protein Voltage-Dependent Anion Channel Is Coupled to the Induction of Apoptosis. *Mol and Cell Biol.* 30(24), 5698-5709.

Keinan, N., Tyomkin, D., Shoshan-Barmatz, V. (2010) Oligomerization of the Mitochondrial Protein Voltage-Dependent Anion Channel Is Coupled to the Induction of Apoptosis. *Mol Cell Biol*. 30(24), 5698-5709.

Kennedy, B., Leblanc, V., Mailman, T., Fice, D., Burton, I., Karakach, T., Karten, B. (2013) Pre-symptomatic activation of antioxidant responses and alterations in glucose and pyruvate metabolism in Niemann-pick type c1-deficient murine brain. PLoS One8:e82685.

Kennedy, B., Madreiter, C., Vishnu, N., Malli, R., Graier, W., Karten, B. (2014) Adaptations of energy metabolism associated with increased levels of

mitochondrial cholesterol in Niemann-Pick type C1-deficient cells. *J Biol Chem.* 289(23), 16278-16289.

Kleene, R., Pfanner, N., Pfaller, R., Link, T., Sebald, W., Neupert, W., Tropschug, M. (1987) Mitochondrial porin of Neurospora-crassa — cDNA cloning, in vitro expression and import into mitochondria. *EMBO J*. 6, 2627-2633.

Kraemer, F., Khor, V., Shen, W., Azhar, S. (2013) Cholesterol ester droplets and steroidogenesis. *Mol Cell Endocrinol*. 371, 15–19.

Kuchinskiene, Z., Carlson, L. (1982) Composition, concentration, and size of low density lipoproteins and of subfractions of very low density lipoproteins from serum of normal men and women*. J Lipid Res*. 23, 762-769.

Kwon, H., Abi-Mosleh, L., Wang, M., Deisenhofer, J., Goldstein, J., Brown, M., Infante, R. (2009) Structure of N-terminal domain of NPC1 reveals distinct subdomains for binding and transfer of cholesterol. *Cell*. 137(7), 1213–1224.

Lacapere, J., Papadopoulos, V. (2003) Peripheral-type benzodiazepine receptor: structure and function of a cholesterol-binding protein in steroid and bile acid biosynthesis. *Steroids*. 68, 569-585.

Laurich, V., Trbovich, A., O'Neill, F., Houk, C., Sluss, P., Payne, A., Donahoe, P., Teixeira, J. (2002) Mullerian inhibiting substance blocks the protein kinase A-induced expression of cytochrome P450 17{α}-hydroxylase/C17–20 lyase mRNA in a mouse Leydig cell line independent of cAMP responsive element binding protein phosphorylation. *Endocrinology*. 143, 3351-3360.

Lee, G., Zheng, Y., Cho, S., Jang, C., England, C., Dempsey, J., Yu, Y., Liu, X., He, L., Cavaliere, P., Chavez, A., Zhang, E., Isik, M., Couvillon, A., Dephoure, N., Blackwell, T., Yu, J., Rabinowitz, J., Cantley, L., Blenis, J. (2017) Post-transcriptional Regulation of De Novo Lipogenesis by mTORC1-S6K1-SRPK2 Signaling. *Cell*. 171(7), 1545-1558.

Létourneau, D., Lorin, A., Lefebvre, A., Frappier, V., Gaudreault, F., Najmanovich, R., Lavigne, P., LeHoux, J. (2012) StAR-related lipid transfer domain protein 5 binds primary bile acids. *J Lipid Res*. 53(12), 2677-1689.

Lin, M., Beal, M. (2006) Mitochondrial dysfunction and oxidative stress in neurodegenerative diseases. *Nature.* 443, 787–795.

Liscum, L., Munn, N. (1999) Intracellular cholesterol transport. *Biochim et Biophys Acta.* 1438, 19-37.

Liu, Y., Guardia-Laguerta, C., Yin, J., Erdjument-Bromage, H., Martin, B., James, M., Jiang, X., Przedborski, S. (2017) The Ubiquitination of PINK1 Is Restricted to Its Mature 52-kDa Form. *Cell Reports.* 20, 30–39.

Lo, Y., Wong, J., Cruz, T. (1996) Reactive oxygen species mediate cytokine activation of c-Jun NH2-terminal kinases. *J Biol Chem*. 271(26), 15703-15707.

Magri, A., Reina, S., De Pinto, V. (2018) VDAC1 as Pharmacological Target in Cancer and Neurodegeneration: Focus on Its Role in Apoptosis. *Front Chem.* 6(108), doi: 10.3389/fchem.2018.00108

Magrì, A., Reina, S., De Pinto, V. (2018) VDAC1 as Pharmacological Target in Cancer and Neurodegeneration: Focus on Its Role in Apoptosis. *Front Chem*. 6(108). doi: 10.3389/fchem.2018.00108.

Marí, M., Caballero, F., Colell, A., Morales, A., Caballeria, J., Fernandez, A., et al. (2006). Mitochondrial free cholesterol loading sensitizes to TNF- and Fas-mediated steatohepatitis. *Cell Metab*. 4, 185–198.

Marí, M., Morales, A., Colell, A., García-Ruiz, C., Fernández-Checa, J. (2009) Mitochondrial Glutathione, a Key Survival Antioxidant. *Antiox Redox Signal.* 11, 2685-2700.

Martin, W., Julia, S., Martin, H. (2004) Mutual amplification of apoptosis by statin-induced mitochondrial stress and doxorubicin toxicity in human rhabdomyosarcoma cells. *Br J Pharmacol.* 143(6), 715-724.

Matsuda, N., Sato, S., Shiba, K., Okatsu, K., Saisho, K., Gautier, C., Sou, Y., Saiki, S., Kawajiri, S., Sato, F., Kimura, M., Komatsu, M., Hattori, N., Tanaka, K. (2010) PINK1 stabilized by mitochondrial depolarization recruits Parkin to damaged mitochondria and activates latent Parkin for mitophagy. *J Cell Biol*. 189, 211–221.

Mauch, D., Nagler, K., Schumacher, S., Goritz, C., Muller, E., Otto, A. (2001) CNS synaptogenesis promoted by glia-derived cholesterol. *Science.* 294, 1354–1357.

Mesmin, B., Maxfield, F. (2009) Intracellular sterol dynamics. *Biochim et Biophys Acta.* 1791, 636-645.

Messina, A., Reina, S., Guarino, F., De Pinto, V. (2012) VDAC isoforms in mammals. *Biochim Biophys Acta*. 1818(6), 1466-1476.

Mihara, K., Sato, R. (1985) Molecular-cloning and sequencing of cDNA for yeast porin, an outer mitochondrial-membrane protein — a search for targeting signal in the primary structure. *EMBO J*. 4, 769-774.

Millard, E., Srivastava, K., Traub, L., Schaffer, J., Ory, D. (2000) Niemann-Pick Type C1 (NPC1) Overexpression Alters Cellular Cholesterol Homeostasis. *J Biol Chem*. 275(49), 38445, 38451.

Montero, J., Morales, A., Llacuna, L., Josep, M., Lluis, Terrones, O., Basanez, G., Antonsson, B., Prieto, J., García-Ruiz, C., Colell, A., Fernández-Checa, J. (2008)

Mitochondrial Cholesterol Contributes to Chemotherapy Resistance in Hepatocellular Carcinoma. *Cancer Res.* 68(13), 5246-5256.

Mukherjee, S., Zha, X., Tabas, I., Maxfield, F. (1998) Cholesterol Distribution in Living Cells: Fluorescence Imaging Using Dehydroergosterol as a Fluorescent Cholesterol Analog. *Biophys J*. 75(4), 1915-1925.

Murtola, T., Visvanathan, K., Artama, M., Vainio, H., Pukkala, E. (2014) Statin use and breast cancer survival: a nationwide cohort study from Finland. *PLoS One.* 9:e110231

Narendra, D., Tanaka, A., Suen, D., Youle, R. (2008) Parkin is recruited selectively to impaired mitochondria and promotes their autophagy. *J Cell Biol*. 183, 795–803.

Narendra, D., Youle, R. (2011) Targeting mitochondrial dysfunction: role for PINK1 and Parkin in mitochondrial quality control. *Antioxid. Redox Signal*. 14, 1929–1938.

Naureckiene, S., Sleat, D., Lackland, H., Fensom, A., Vanier, M., Wattiaux, R., Jadot, M., Lobel, P. (2000) Identification of HE1 as the Second Gene of Niemann-Pick C. *Science.* 290

Ness, G., Zhao, Z., Wiggins, L. (1994) Insulin and glucagon modulate hepatic 3-hydroxy-3-methylglutaryl-coenzyme A reductase activity by affecting immunoreactive protein levels. *J Biol Chem.* 269(46), 29168-29172.

Nir, A., Ben-Hail, D., Shoshan-Barmatz, V. (2012) Mediation of the Antiapoptotic Activity of Bcl-xL Protein upon Interaction with VDAC1 Protein. *J Biol Chem*. 287(27), 23152–23161.

Nohturfft, A., Brown, M., Goldstein, J. (1998) Topology of SREBP cleavage-activating protein, a polytopic membrane protein with a sterol-sensing domain. *J Biol Chem.* 273, 17243–17250.

Norton, W., Autilo, L. (1966) The lipid composition of purified bovine brain myelin. *J Neurochem*. 13, 213-222.

Olaioye, M., Vehring, S., Muller, P., Herrmann, A., Schiller, J., Thiele, C., …, Pomorski, T. (2005) STARD10, a START domain protein overexpressed in breast cancer, functions as a phospholipid transfer protein. *J Biol Chem*. 280(29), 27436-27442.

Ory, D. (2004) The Niemann-pick disease genes; regulators of cellular cholesterol homeostasis. *Trends Cardiovasc Med.* 14, 66-72.

Pan, J., Tristram-Nagle, S., Nagle, J. (2009) Effect of cholesterol on structural and mechanical properties of membranes depends on lipid chain saturation. *Phys Rev*. doi: 10.1103/PhysRevE.80.021931.

Patel, M., and Roche, T. (1990) Molecular biology and biochemistry of pyruvate dehydrogenase complexes. *FASEB J*. 4, 3224–3233.

Patterson, M., Vanier, M., Suzuki, K., Morris, J., Carstea, E., Neufeld, E., Blanchette-Mackie, J., Pentchev P. (2001) Niemann-Pick Disease Type C: a lipid trafficking disorder. The Metabolic and Molecular Bases of Inherited Disease. Scriver C., Beaudet A., Sly W., Valle D., editors. McGraw-Hill, New York. 3611–3633.

Patterson, M., Vecchio, D., Prady, H., Abel, L., Wraith, J. (2007) Miglustat for treatment of Niemann-Pick C disease: a randomized controlled study. *Lancet Neurol*. 6(9), 765-772.

Pike, L. (2003) Lipid rafts: bringing order to chaos. *J Lipid Res*. 44: 655-667.

Reinhart, M., Billheimer, J., Faust, J., Gaylor, J. (1987) Subcellular localization of the enzymes of cholesterol synthesis and metabolism in rat liver. *J Biol Chem*. 262(20) 9649-9655.

Rennert, H., Fischer, R., Alvarez, J., Trzaskos, J., Strauss, J. (1990) Generation of Regulatory Oxysterols: 26-Hydroxylation of Cholesterol by Ovarian Mitochondria. *Endocrinology*. 127(2), 738-746.

Rieusset, J. (2018) The role of endoplasmic reticulum-mitochondria contact sites in the control of glucose homeostasis: an update. *Cell Death Dis.* 9(388). DOI 10.1038/s41419-018-0416-1

Romanowski, M., Soccio, R., Breslow, J., Burley, S. (2002) Crystal structure of the *Mus musculus* cholesterol-regulated START protein 4 (StarD4) containing a StAR-related lipid transfer domain. *PNAS*. 99(10) 6949-6954.

Rone, M., Midzak, A., Issop, L., Rammouz, G., Jagannathan, S., Fan, J., Ye, X., Blonder, J., Veenstra, T., Papadopoulos, V. (2012) Identification of a Dynamic Mitochondrial Protein Complex Driving Cholesterol Import, Trafficking, and Metabolism to Steroid Hormones. *Mol Endocrinol*. 26(11), 1868-1882.

Malena B. Rone, Andrew S. Midzak, Leeyah Issop, Georges Rammouz, Sathvika Jagannathan, Jinjiang Fan, Xiaoying Ye, Josip Blonder, Timothy Veenstra, and Vassilios

Rostovtseva, T., Colombini, M. (1996) ATP flux is controlled by a voltage-gated channel from the mitochondrial outer membrane. *J Biol Chem*. 271, 28006-28008.

Sabers, C., Martin, M., Brunn, G., Williams, J., Dumont, F., Wiederrecht, G., Abraham, R. (1995) Isolation of a protein target of the FKBP12-rapamycin complex in mammalian cells. *J Biol Chem*. 270(2), 815-822.

Sakakura, Y., Shimano, H., Sone, H., Takahashi., A., Inoue., K, Toyoshima, H., Suzuki, S., Yamada, N. (2001) Sterol regulatory element-binding proteins induce an entire pathway of cholesterol synthesis. *Biochem Biophys Res Com.* 286, 176-183.

Savic, D., Partridge, C., Newberry, K., Smith, S., Meadows, S., Roberts, B., Mackiewicz, M., Mendenhall, M., Myers, R. (2015) CETCh-seq: CRISPR epitope tagging ChIP-seq of DNA-binding proteins. *Genome Res*. 25(10), 1581-1589.

Sever, N., Yang, T., Brown, M., Goldstein, J., DeBose-Boyd (2003) Accelerated degradation of HMG CoA reductase mediated by binding of Insig-1 to its sterol sensing domain. *Molecular Cell*. 11, 25-33.

Sever, N., Yang, T., Brown, M., Goldstein, J., Debose-Boyd, R. (2003) Accelerated degradation of HMG CoA reductase mediated by binding of insig-1 to its sterol-sensing domain. *Mol Cell.* 11(1), 25-33.

Silvius, J. (2003) Role of cholesterol in lipid raft formation: lessons from lipid model systems. *Biochim Biophys Acta.* 1610(2), 174-183.

Simona F., Alfonso, R., Casa, R., Giudice, E., Bruschini, D., …, Andria, G. (2015) Long term follow-up to evaluate the efficacy of miglustat treatment in Italian patients with Niemann-Pick disease type C. *Orphanet*. 10(22).

Soccio, R., Adams, R., Maxwell, K., Breslow, J. (2005) Differential gene regulation of Stard4 and STARD5 cholesterol transfer proteins. *J Biol Chem.* 280(19), 19410-19418.

Sokol, J., Blanchette-Mackies, J., Kruth, H., Dwyer, N., Amende, L., Butler, J., Robinson, E., Patel, S., Brady, R., Comly, M., Vanier, M., Pentchev, P. (1988) Lysosomal accumulation and defective intracellular mobilization of low density lipoprotein cholesterol. *J Biol Chem*. 263(7), 3411-3417.

Springer, W., Kahle, P. (2011) Regulation of PINK1-Parkin-mediated mitophagy. *Autophagy*. 7, 266–278.

Stacpoole, P., Felts, J. (1970) Diisopropylammonium dichloroacetate (DIPA) and sodium dichloracetate (DCA): Effect on glucose and fat metabolism in normal and diabetic tissue. *Metabolism*. 19(1), 71–78.

Streicher, R., Kotzka, J., Müller-Wieland, D., Siemeister, G., Munck, M., Avci, H., Krone, W. (1996) SREBP-1 Mediates Activation of the Low Density Lipoprotein Receptor Promoter by Insulin and Insulin-like Growth Factor-I. *J Biol Chem.* 271, 7128-7133.

Sun, Y., Vashisht, A., Tchieu, J., Wohlschlegel, J., Dreier, L. (2012) Voltage-dependent anion channels (VDACs) recruit Parkin to defective mitochondria to promote mitochondrial autophagy. *J Biol Chem*. 287(48), 40652-40660.

Szabadkai, G., Bianchi, K., Várnai, P., De Stefani, D., Wieckowski, M., Cavagna, D., Nagy, A., Balla, T., Rizzuto, R. (2006). Chaperone-mediated coupling of endoplasmic reticulum and mitochondrial Ca2+ channels. *J Cell Biol*. 175, 901–911.

Szabadkai, G., Bianchi, k., Várnai, P., De Stefani, D., Wieckowski, M., Cavagna, D., Nagy, A., Balla, T., Rizzuto, R. (2006) Chaperone-mediated coupling of endoplasmic reticulum and mitochondrial Ca2+ channels. *J Cell Biol.* 175(6), 901-911.

Tonelli, C., Chio, I., Tuveson, D. (2018) Transcriptional Regulation by Nrf2. *Antioxid Redox Signal.* 29(17), 1727-1745.

Torres, S., Balboa, E., Zanlungo, S., Enrich, C., Garcia-Ruiz, C., Fernandez-Checa, J. (2017) Lysosomal and mitochondrial liasons in Niemann-Pick Disease. *Front Physiol* 8(982), doi: 10.3389/fphys.2017.00982

Ujwal, R., Cascio, D., Colletier, J., Faham, S., Zhang, J., Toro, L., Ping, P., Abramson, J. (2008) The crystal structure of mouse VDAC1 at 2.3 Å resolution reveals mechanistic insights into metabolite gating. *PNAS.* 105(46), 17742-17747.

van Meer, G., Voelker, D., Feigenson, G. (2008) Membrane lipids: where they are and how they behave. *Mol Cell Biol*. 9, 112-124.

Vance, J. (2012) Dysregulation of cholesterol balance in the brain: contribution to neurodegenerative diseases. *Dis Models Mech*, 5, 746-755.

Vander Heiden, M., Chandel, N., Li, X., Schumacker, P., Colombini, M., Thompson, C. (2000) Outer mitochondrial membrane permeability can regulate coupled respiration and cell survival. *Proc Natl Acad Sci USA*. 97, 4666–4671.

Vanier, M., Millat, G. (2003) Niemann-Pick disease type C. *Clin Genet.* 64, 269-281.

Vanier, M., Rodriguez-Lafrasse, C., Rousson, R., Duthel, S., Harzer, K., Pentchev, P., Revol, A,, Louisot, P. (1991) Type C Niemann-Pick disease: biochemical aspects and phenotypic heterogeneity. *Dev Neurosci.* 12, 307–314.

Vives-Bauza, C., Zhou, C., Huang, Y., Cui, M., de Vries, R., Kim, J., May, J., Tocilescu, M., Liu, W., Ko, H., Magrané, J., Moore, D., Dawson, V., Grailhe, R., Dawson, T., Li, C., Tieu, K., Przedborski, S. (2010) PINK1-dependent recruitment of Parkin to mitochondria in mitophagy. *Proc Natl Acad Sci.* 107, 378–383.

Warburg, O., Wind, F., Negelein, E. (1927) The metabolism of tumors in the body. *J Gen Physiol*. 8, 519–530.

Weiser, B., Salari, R., Eckenhoff, R., Brannigan, G. (2014) Computational Investigation of Cholesterol Binding Sites on Mitochondrial VDAC. *J Phys Chem.* 118(33), 9852-9860.

Whitehouse, S., Cooper, R., Randle, P. (1974) Mechanism of activation of pyruvate dehydrogenase by dichloroacetate and other halogenated carboxylic acids. *Biochem J*. 141(3):761–774.

Wilhelm, L., Wendling, C., Védie, B., Kobayashi, T., Chenard, M., Tomasetto, C., Drin, G., Alpy, F. (2017) STARD3 mediates endoplasmic reticulum-to-endosome cholesterol transport at membrane contact sites. *EMBO J*. 36(10), 1412-1433.

Wirtz. (1991) Phospholipid transfer proteins. *Annu Rev Biochem*. 60, 73-99.

Wolf, B., Schuler, M., Echeverri, F., Green, D. (1999) Caspase-3 Is the Primary Activator of Apoptotic DNA Fragmentation via DNA Fragmentation Factor-45/Inhibitor of Caspase-activated DNase Inactivation. *J Biol Chem*. 274(43), 30651-30656.

Xiao, B., Goh, J., Xiao, L., Xian, H., Lim, K., Liou, Y. (2017) Reactive oxygen species trigger Parkin/PINK1 pathway-dependent mitophagy by inducing mitochondrial recruitment of Parkin. *J Biol Chem*. 292(40), 16697-16708.

Xu, S., Benoff, B., Liou, H., Lobel, P., Stock, A. (2007) Structural basis of sterol binding by NPC2, a lysosomal protein deficient in Niemann-Pick type C2 disease. *J Biol Chem*. 282(32), 23525–23531.

Yang, T., Espenshade, P., Wright, M., Yabe, D., Gong, Y., Aebersold, R., Goldstein, J., Brown., M. (2002) *Cell*. 110, 489-500.

Zalk, R., Israelson, A., Garty, E., Azoulay-Zohar, H., Shoshan-Barmatz, V. (2005) Oligomeric states of the voltage-dependent anion channel and cytochrome c release from mitochondria. *Biochem J*. 386, 73–83.

Zehmer, J., Huang, Y., Peng, G., Pu, J., Anderson, R., Liu, P. (2009) A role for lipid droplets in inter-membrane lipid traffic. *Proteomics* 9, 914–921.

Zervas, M., Somers, K., Thrall, M., Walkley, S. (2001) Critical role for glycosphingolipids in Niemann-Pick disease type C. *Curr Biol.* 11(16), 1283-1287.

Zhou, Q., Lam, P., Han, D., Cadenas, E. (2009) Activation of C-Jun-N-Terminal Kinase and Decline of Mitochondrial Pyruvate Dehydrogenase Activity during Brain Aging. *FEBS Lett*. 583, 1132-1140.

APPENDIX A: PLASMID MAPS

pLenti CMV OMM YFP FRB P2A mCherry FKBP STARD4

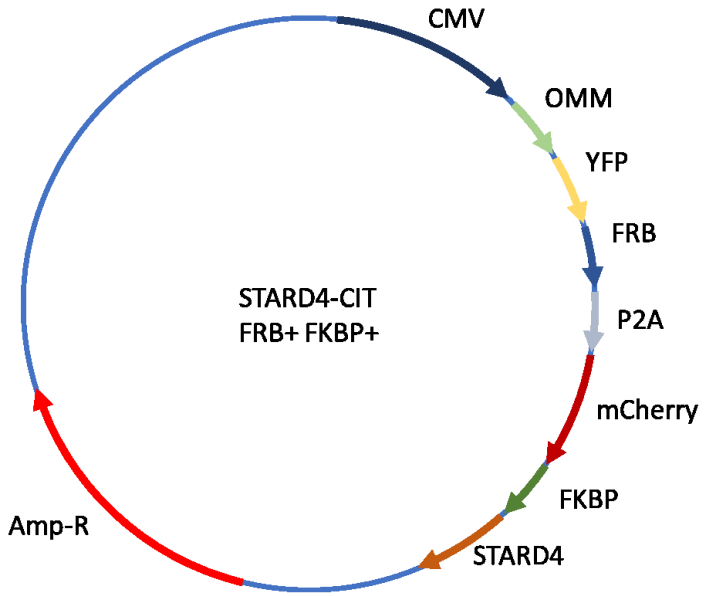

pLenti CMV OMM YFP P2A mCherry FKBP STARD4

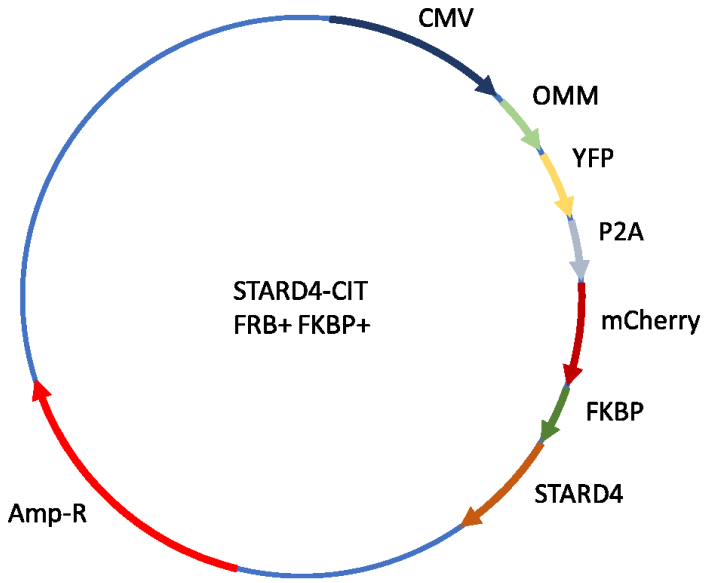

pLenti CMV OMM YFP FRB P2A mCherry STARD4

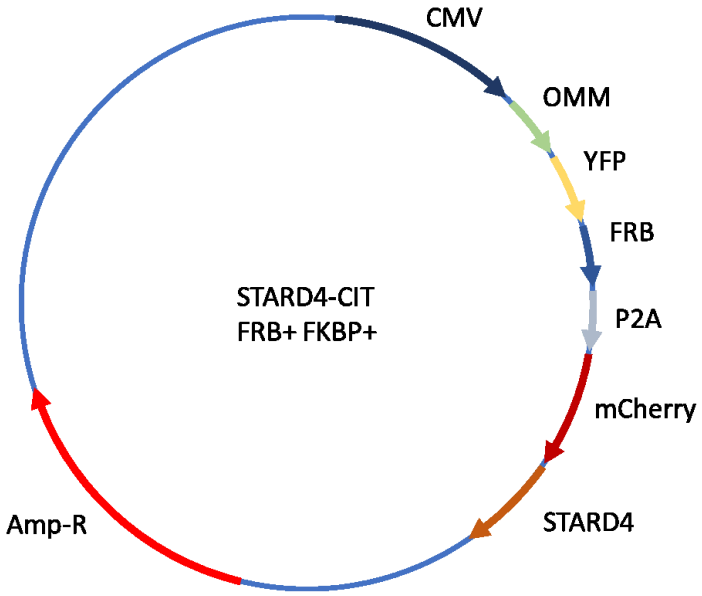

pLenti CMV OMM GlySer V5 STARD4 P2A Clover

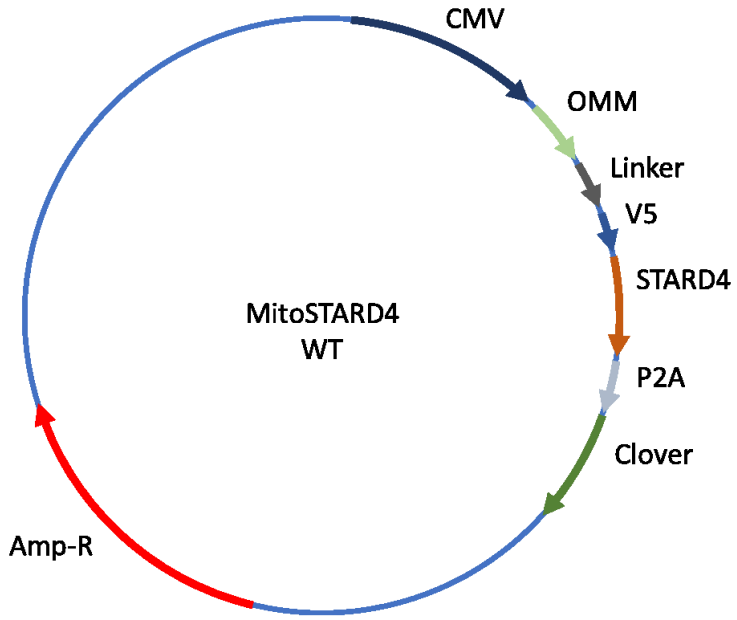

pLenti CMV OMM GlySer V5 STARD4-W108D P2A Clover

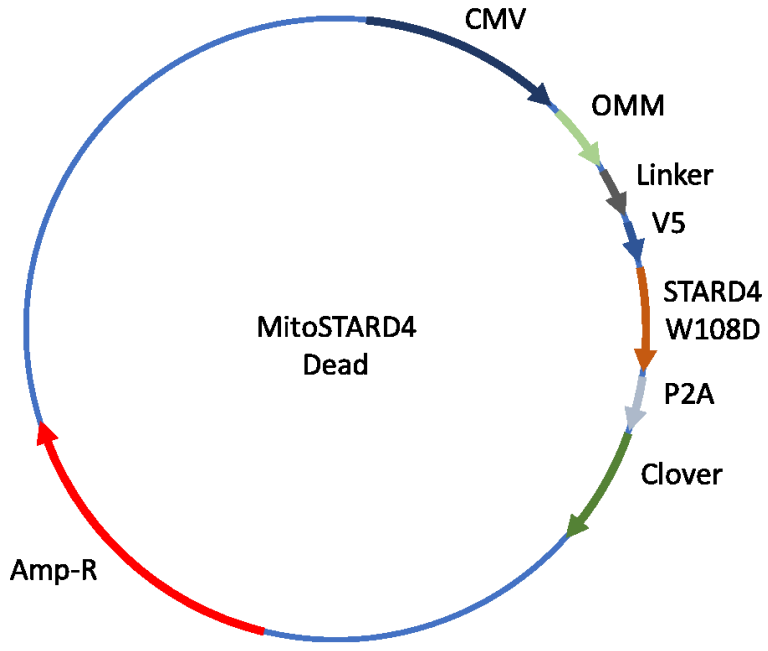

APPENDIX B: VDAC1 CRISPR EDIT SEQUENCE

Sequence of the last exon of CHO VDAC1 gene with CRISPR insert sequence (grey).

29282 - GTA TCA AAC TGA CGC TGT CAG CTC TGC TGG ACG GCA AGA ACG TCA ATG

CGG GTG GCC ACA AAC TAG GAC TCG GAC TGG AAT TTC AAG CAG GGA GCG GAG GAG

GTT CCG GTG GAG GTG GTT CTG GAG ATT ACA AGG ATG ACG ACG ATA AGG GCG ATT

ACA AGG ATG ACG ACG ATA AGG GAG ATT ACA AGG ATG ACG ACG ATA AGG TTT CAG

GAA GCG GAG CTA CTA ACT TCA GCC TGC TGA AGC AGG CTG GAG ACG TGG AGG AGA

ACC CTG GAC CTG GAT CGT TTC GCA TGA TTG AAC AAG ATG GAT TGC ACG CAG GTT

CTC CGG CCG CTT GGG TGG AGA GGC TAT TCG GCT ATG ACT GGG CAC AAC AGA CAA

TCG GCT GCT CTG ATG CCG CCG TGT TCC GGC TGT CAG CGC AGG GGC GCC CGG TTC

TTT TTG TCA AGA CCG ACC TGT CCG GTG CCC TGA ATG AAC TGC AGG ACG AGG CAG

CGC GGC TAT CGT GGC TGG CCA CGA CGG GCG TTC CTT GCG CAG CTG TGC TCG ACG

TTG TCA CTG AAG CGG GAA GGG ACT GGC TGC TAT TGG GCG AAG TGC CGG GGC AGG

ATC TCC TGT CAT CTC ACC TTG CTC CTG CCG AGA AAG TAT CCA TCA TGG CTG ATG

CAA TGC GGC GGC TGC ATA CGC TTG ATC CGG CTA CCT GCC CAT TCG ACC ACC AAG

CGA AAC ATC GCA TCG AGC GAG CAC GTA CTC GGA TGG AAG CCG GTC TTG TCG ATC

AGG ATG ATC TGG ACG AAG AGC ATC AGG GGC TCG CGC CAG CCG AAC TGT TCG CCA

GGC TCA AGG CGC GCA TGC CCG ACG GCG AGG ATC TCG TCG TGA CCC ATG GCG ATG

CCT GCT TGC CGA ATA TCA TGG TGG AAA ATG GCC GCT TTT CTG GAT TCA TCG

ACT GTG GCC GGC TGG GTG TGG CCG ACC GCT ATC AGG ACA TAG CGT TGG

CTA CCC GTG ATA TTG CTG AAG AGC TTG GCG GCG AAT GGG CTG ACC GCT

TCC TCG TGC TTT ACG GTA TCG CCG CTC CCG ATT CGC AGC GCA TCG CCT

TCT ATC GCC TTC TTG ACG AGT TCT TCT GAT TCG AAC ATC